

Irisin attenuates acute lung injury by suppressing the pyroptosis of alveolar macrophages

ZHUOXIAO HAN^{1,2*}, JIAO MA^{1*}, YING HAN³, GUANLI YUAN², RUI JIAO¹ and AIHONG MENG¹

¹Department of Respiratory and Critical Care Medicine, The Second Hospital of Hebei Medical University, Shijiazhuang, Hebei 050000; Departments of ²Respiratory and Critical Care Medicine, and ³Neurosurgery, The First Hospital of Qinhuangdao, Qinhuangdao, Hebei 066000, P.R. China

Received November 23, 2022; Accepted February 22, 2023

DOI: 10.3892/ijmm.2023.5235

Abstract. Irisin is a hormone-like myokine that regulates cell signaling pathways and exerts anti-inflammatory effects. However, the specific molecular mechanisms involved in this process are currently unknown. The present study explored the role and mechanisms underlying the functions of irisin in alleviating acute lung injury (ALI). The present study used MH-S, an established murine alveolar macrophage-derived cell line, and a mouse model of lipopolysaccharide (LPS)-induced-ALI to examine the efficacy of irisin against ALI *in vitro* and *in vivo*, respectively. Fibronectin type III repeat-containing protein/irisin was expressed in the inflamed lung tissue, but not in normal lung tissue. Exogenous irisin reduced alveolar inflammatory cell infiltration and pro-inflammatory factor secretion in mice following LPS stimulation. It also inhibited the polarization of M1-type macrophages and promoted the repolarization of M2-type macrophages, thus reducing the LPS-induced production and secretion of interleukin (IL)-1 β , IL-18 and tumor necrosis factor- α . In addition, irisin reduced the release of the molecular chaperone heat shock protein 90 (HSP90), inhibited the formation of nucleotide-binding and oligomerization domain-like receptor protein 3 (NLRP3) inflammasome complexes, and decreased the expression of caspase-1 and the cleavage of gasdermin D (GSDMD), leading to reduced pyroptosis and the accompanying inflammation. On the whole, the findings of the present study demonstrate that irisin attenuates ALI by inhibiting the HSP90/NLRP3/caspase-1/GSDMD signaling pathway,

reversing macrophage polarization and reducing the pyroptosis of macrophages. These findings provide a theoretical basis for understanding the role of irisin in the treatment of ALI and acute respiratory distress syndrome.

Introduction

Acute lung injury (ALI) is characterized by the exudation of large quantities of inflammatory fluid, the infiltration of inflammatory cells, the severe destruction of alveolar structures, remodeling, lung hemorrhage, edema, fibrosis and decreased alveolar compliance. Acute respiratory distress syndrome (ARDS) is an extreme form of ALI, with a fatality rate as high as 30-40% (1). Pyroptosis is a form of inflammatory programmed cell death (2) triggered by pathogenic infection, and causes local as well as systemic inflammation or septic shock (3). The pyroptosis pathways include the caspase-1-dependent classical pathway and caspase-11/4/5 dependent non-canonical pathway. Pyroptosis, characterized by pore formation in the plasma membrane, cell swelling and the rupture of the plasma membrane, occurs rapidly and is accompanied by the release of multiple pro-inflammatory factors (4). Gasdermins (GSDMs), the family of pore-forming proteins that include GSDM A, B, C, D, E and autosomal recessive deafness type 59 (DFNB59) (4), play a critical role in pyroptosis, which is also referred to as GSDM-mediated necrosis (3,4). Of these GSDM proteins, the cleavage of GSDMD, known as the pyroptosis execution protein, has been extensively studied. After receiving inflammatory stimuli from the cell, the nucleotide-binding and oligomerization domain-like receptor protein 3 (NLRP3) inflammasome activates caspase-1, which then cleaves pro-interleukin (IL)-1 β , pro-IL-18 and GSDMD. The cleavage separates the N-terminal pore-forming domain of GSDMD from its C-terminal repressive domain. The pore-forming domain oligomerizes and creates holes in the cytoplasmic membrane, resulting in the release of cellular contents, which induce a robust inflammatory response (3-5).

Alveolar macrophages (AMs) account for ~95% of alveolar leukocytes (6) and affect the development of both infection-induced and non-infectious ALI by synthesizing and releasing several inflammatory mediators (7,8). Previous studies have confirmed that AM cell death significantly affects

Correspondence to: Dr Aihong Meng, Department of Respiratory and Critical Care Medicine, The Second Hospital of Hebei Medical University, 215 Heping West Road, Shijiazhuang, Hebei 050000, P.R. China
E-mail: mengaihong_med@126.com

*Contributed equally

Key words: irisin, acute lung injury, pyroptosis, molecular chaperone heat shock protein 90, nucleotide-binding oligomerization domain-like receptor 3

the progression of lung inflammation (9-11). In a previous study, a lipopolysaccharide (LPS)-induced septic lung injury survey revealed that LPS activated the NLRP3 inflammasome through the TLR4/MyD88/NF- κ B signaling pathway and promoted the secretion of IL-1 β by AM; LPS enhanced the sensitivity of AM to IL-1 β , resulting in AM pyroptosis (12). That previous study also demonstrated that AM pyroptosis induced the migration of neutrophils into the lungs, increased IL-6, tumor necrosis factor (TNF)- α , and IL-1 β production in alveoli, and aggravated the histological manifestations of lung injury (12). Therefore, inhibiting AM pyroptosis may be a promising therapeutic strategy for reducing ALI.

Heat shock protein (HSP)90 is a well-known molecular chaperone belonging to the HSP family. As a client protein of HSP90, the assembly and stability of the NLRP3 inflammasome are affected by HSP90 (13,14). HSP90 binds NLRP3, which regulates inflammasome activation and IL-1 β secretion (13,15,16). Without HSP90, NLRP3 can be misfolded and degraded by proteases (17,18). HSP90 inhibitors have previously been shown to reduce the expression of HSP90 in a time- and dose-dependent manner and to significantly attenuate the LPS- and nigericin-induced pyroptosis of human monocytic leukemia (THP-1) cells (2), suggesting that HSP90 is a promising target for the treatment of inflammation. Compared to other HSP90 inhibitors, tanespinmycin (17-AAG) has a lower cytotoxic effect; it significantly reduces the production of active caspase-1 and inhibits NLRP3 expression (2).

Irisin is a muscle- or lipid-derived cytokine expressed in the heart, brain, ovaries, testes, kidneys, stomach and liver (19,20), but not in the lungs. Irisin, produced by the hydrolysis of fibronectin type III repeat-containing protein (FNDC5), reduces oxidative stress and has neuroprotective, anti-inflammatory and anticancer properties. It also plays a biological role in several cellular signaling pathways (20). FNDC5/irisin reduces inflammation and M1 macrophage polarization by regulating the 5' AMP-activated protein kinase pathway (21). As demonstrated in a previous study, following irisin pre-treatment, the stimulation of RAW264.7 macrophages with LPS significantly decreased T-lymphoid receptor and myeloid differentiation primary response protein 88 levels. It also decreased the phosphorylation of nuclear factor κ B (NF- κ B) and inhibited the release of critical pro-inflammatory cytokines, such as IL-6, TNF- α and IL-1 β (22). Shao *et al* (23) found that irisin inhibited the activation of NF- κ B and phosphorylated (p-) NF- κ B by LPS, and attenuated inflammatory responses and pathological changes in cells within an LPS-induced mouse lung injury model, indicating that irisin may be a treatment agent for ALI (23).

The present study aimed to examine the protective role of irisin in ALI and to elucidate its underlying mechanisms of action, in an aim to identify novel targets for the treatment of ALI/ARDS.

Materials and methods

Reagents. Irisin was purchased from Cayman Chemical Company. LPS (*Escherichia coli* 0111: B4) was purchased from MilliporeSigma. MCC950 (cat. no. HY-12815) and 17-N-allylamino-17-demethoxygeldanamycin (17-AAG, cat. no. M2320-01) were purchased from MedChemExpress.

The immunohistochemistry kit (cat. no. PV-9000) was purchased from Beijing Zhongshan Jinqiao Biotechnology Co., Ltd. Ethanol and dimethyl benzene were purchased from Tianjin Yongda Chemical Reagent Co., Ltd. The hematoxylin and eosin (H&E) Stain Kit (cat. no. G1120) and paraffin wax were purchased from Beijing Solarbio Science & Technology Co., Ltd. Primers used for reverse transcription-quantitative PCR (RT-qPCR) primers were synthesized by Sangon Biotech Co., Ltd.

Animals. C57BL/6J mice (n=48, 24 male and 24 female mice; aged 6-8 weeks and weighing 18-22 g) were purchased from Beijing Weitong Lihua Experimental Animal Technology Co. Ltd. All mice were raised and maintained at the Hebei Medical University Animal Care Center (Shijiazhuang, China) under a standard SPF facility. Animal experimental and handling procedures were approved by the Ethics Committee of the Second Hospital of Hebei Medical University (Approval no: 2022-AE008, 28.2.2022). All efforts were made to minimize the suffering of the animals, and conformed with the National Institutes of Health guide for the care and use of laboratory animals (24). All experiments were performed under standard growth conditions as follows: 40-60% relative humidity, room temperature (23-25°C) and a 12-h light/dark cycle, with 5 mice per cage with cleaned bedding and *ad libitum* access to food and water. The mice were allowed to acclimatize to the laboratory conditions for at least 7 days prior to the commencement of the experiments. Humane endpoints associated with infection in the experiment were compliant with the Guidelines for the Assessment of Humane Endpoints in Animal Experiments (RB/T 173-2018, in Chinese), as follows: The animal body temperature decreases by >4-6°C; animal weight loss of 10-20%; reduced animal activity, lethargy and other physiological and behavioral changes up to 24 h. None of the mice used in the experiment exhibited any of these endpoints.

Establishment of mouse model of LPS-induced of ALI and mouse grouping. The mice (n=48) were randomly divided into eight groups as follows: i) The control (Con; 0.05 ml of 0.9% saline injected intratracheally); ii) low LPS (LPS; 2 mg/kg LPS injected intratracheally); iii) high LPS (LPS-H; 4 mg/kg LPS injected intratracheally); iv) LPS + low irisin (LPS + IR-L; 0.25 mg/kg irisin injected in the caudal vein 0.5 h before 2 mg/kg LPS administration); v) LPS + high irisin (LPS + IR; 0.5 mg/kg irisin injected 0.5 h prior to the 2 mg/kg LPS administration); vi) low MCC950 (LPS + M-L; 25 mg/kg of MCC950 injected intraperitoneally 12 h before the 2 mg/kg LPS administration); vii) high MCC950 (LPS + M; 50 mg/kg of MCC950 injected intraperitoneally 12 h before the 2 mg/kg LPS administration); and viii) LPS + dexamethasone (Dex, CSPC Pharmaceutical Group Ltd; LPS + Dex; 0.5 mg/kg of Dex injected intraperitoneally 0.5 h before the 2 mg/kg LPS administration). MCC950, an inhibitor of the NLRP3 inflammasome and Dex were used as the positive controls.

Preparation of bronchoalveolar lavage fluid (BALF). After 24 h, all mice (n=48) were euthanized by deep anesthesia with pentobarbital sodium and subjected to rapid bloodletting. The mice were weighed before anesthesia and the average weight

was 20.7 g. A 1% pentobarbital sodium solution (35 mg/kg) was prepared and the mice were injected intraperitoneally for deep anesthesia. The orbital artery of the mouse was then selected to perform rapid bloodletting, completing the euthanasia of the mice (the bloodletting volume was 0.7-1 ml). If the mouse did not die after bleeding, it was euthanized by cervical dislocation as soon as possible. The criteria for confirming the death of the mice were as follows: No breathing, no pulse and no heartbeat in the thoracic cavity of the mouse for >5 min; the corneal reflex of the animal disappeared; the pupils dilated; and the nerve reflexes disappeared. Blood samples were then collected for use in further experimental procedures. The mice were immobilized on the operating table and the skin and muscles were cut in the front of the neck of the mice to expose the trachea. A 22G Disposable Vein Detaining Needle (BD Biosciences) was inserted into the primary airway, and 500 μ l saline solution were then injected in three batches. BALF was collected by injection and withdrawal three times. The BALF samples were mixed, and 50 μ l of the mixed sample were used to count the white blood cell (WBC) number using a hemocytometer (Countess 3, Thermo Fisher Scientific, Inc.). The remaining BALF was maintained at -80°C for use in cytokine analysis for cell counting and detecting cytokine levels.

Histopathological evaluation and immunohistochemistry. Fresh tissue samples were collected from the inferior lobe of the left lung and fixed with 4% paraformaldehyde for 24 h. The samples were dehydrated using a series of ethanol, cleared using dimethyl benzene, and embedded in paraffin wax. Paraffin-embedded sections with a thickness of 4 μ m were cut and stained with hematoxylin and eosin staining for 1 min at room temperature. The pathological changes in the lung tissues were observed using a light microscope (Zeiss Scope.A1; Zeiss AG; x200 magnification). FNDC5 expression was detected using immunohistochemistry. Briefly, following deparaffinization and rehydration, antigen retrieval was performed by heat-mediated antigen retrieval with sodium citrate buffer (cat. no. DNS-0811, MXB Biotechnologies, pH 9.0) at 98°C for 15 min. Subsequently, the sections were stained with anti-FNDC5 (1:100; cat. no. BS-8486R, BIOSS) primary antibody at 4°C overnight. Subsequently, at room temperature, the sections were incubated with biotin-labeled goat anti-rabbit IgG (1:50; cat. no. SP KIT-C2, MXB Biotechnologies) for 30 min, followed by a reaction with diaminobenzidine (cat. no. DAB-2031, MXB Biotechnologies) for 3-5 min. Images were observed under an optical microscope (Zeiss Scope.A1; Zeiss AG; x200 magnification).

Cells and cell culture. The mouse AM-derived cell line, MH-S, was purchased from ATCC (cat. no. BFN60807584) and cultured in RPMI-1640 medium (MilliporeSigma). The cells were supplemented with 10% fetal bovine serum (Gibco; Thermo Fisher Scientific, Inc.) and 1% penicillin-streptomycin solution (Thermo Fisher Scientific, Inc.) and incubated at 37°C under a 5% CO₂ and 95% O₂ atmosphere.

Cell proliferation assay. The MH-S cells were plated in 96-well plates at a density of 1x10⁴ cells per well for 24 h and then grown for a further 24 h in various concentrations of LPS (0.01, 0.1, 1, 10 and 100 μ g/ml), irisin (100, 200 and 400 ng/ml),

or 17-AAG (50, 100 and 200 ng/ml). 17-AAG, an inhibitor of the HSP90 inflammasome, was used as a positive control. Cell viability was estimated using the Cell Counting Kit-8 assay (Dalian Meilun Biotechnology, Co., Ltd.) according to the manufacturer's instructions.

Morphological changes in the MH-S cells. The MH-S cells in the logarithmic growth phase were seeded in 6-well plates at 2x10⁵ cells per well. The cells were divided into four groups as follows: The control (Con; saline solution 10 μ l), LPS (LPS 10 μ g/ml), LPS + irisin (LPS + IR; 10 μ g/ml LPS and 200 ng/ml IR) and the LPS + 17-AAG (LPS + 17; 10 μ g/ml LPS and 100 ng/ml 17-AAG) groups were set up. Irisin and 17-AAG were combined with serum-free RPMI-1640 medium and added to the cells 2 h prior to LPS stimulation. Morphological changes in the cells were observed using the PE Perkin Elmer Operetta CLS system 4 h following LPS stimulation.

Cell pyroptosis assay. To evaluate cell pyroptosis, the MH-S cells were plated in six-well plates (2x10⁵ cells per well) for 24 h. The cells were treated and grouped as described above. Following 4 h of LPS treatment, the MH-S cells were washed thrice with PBS after being incubated with Calcein AM and 7-aminoactinomycin D (7-AAD) using the Live/Membrane Damage Cell Staining kit (cat. no. BB-41272, BestBio), following the manufacturer's instructions. The cells were incubated in the dark at 4°C for 15-30 min, washed with PBS, and then analyzed under a fluorescence microscope (Zeiss Axio Vert.A1, Zeiss AG; x400 magnification).

Immunofluorescence assays. The lung tissue sections were dewaxed, and cell samples were fixed with 4% paraformaldehyde for 15 min. The samples were permeabilized with 0.3% Triton X-100 for 10 min and blocked using 1% bovine serum albumin (BSA) for 1 h at room temperature. Subsequently, the samples were incubated overnight at 4°C with anti-CD68 (1:100), anti-CD206 (1:200), or anti-inducible nitric oxide synthase (iNOS, 1:200) primary antibodies. The same method was applied as that described above for the immunofluorescence experiments of macrophage pyroptosis (CD80, 1:100; and GSDMD, 1:200). Following incubation, the samples were washed twice with PBS and incubated in the dark for 2 h with fluorescein-labeled secondary antibodies. Finally, the nuclei were stained with 4',6-diamidino-2-phenylindole (DAPI; RS0029, Report Biotech, China) for 5 min at room temperature. Antibodies against CD68 (cat. no. EM1706-11) and CD80 (cat. no. M1007-10) were purchased from HUABIO. Antibodies against CD206 (cat. no. 18704-1-AP), iNOS (cat. no. 22226-1-AP) and GSDMD (cat. no. 20770-1-AP) were purchased from Proteintech Group, Inc. Secondary antibodies used for immunofluorescence were purchased from the Beyotime Institute of Biotechnology (Alexa Fluor 488-labeled goat anti-mouse IgG, cat. no. A0428; Alexa Fluor 647-labeled goat anti-rabbit IgG, cat. no. A0468), diluted at a ratio of 1:500. Immunofluorescence images were captured using an Axio Vert.A1 fluorescence microscope (Zeiss AG; x400 magnification).

Enzyme-linked immunosorbent assay (ELISA). For the *in vivo* experiments, BALF and blood samples were centrifuged at 3,500 x g at 4°C for 10 min and the cell culture supernatant was

Table I. Primers used for the reverse transcription-quantitative polymerase chain reaction in the present study.

Gene	Forward primer (5'→3')	Reverse primer (3'→5')
<i>NLRP3</i>	GCCGTCTACGTCTTCTTCCTTTCC	CATCCGCAGCCAGTGAACAGAG
<i>HSP90</i>	CTCAGTCTGGAGATGAGATGAC	CAGTCATATACACCACCTCGAA
<i>Caspase-1</i>	AGAGGATTTCTTAACGGATGCA	TCACAAGACCAGGCATATTCTT
<i>GSDMD</i>	CTAGCTAAGGCTCTGGAGACAA	GATTCCTTTTCATCCCAGCAGTC
<i>IL-1β</i>	CACTACAGGCTCCGAGATGAACAAC	TGTCGTTGCTTGGTTCTCCTTGATC
<i>IL-18</i>	AGACCTGGAATCAGACAACCTT	TCAGTCATATCCTCGAACACAG
<i>TNF-α</i>	ATGTCTCAGCCTCTTCTCATTC	GCTTGTCACTCGAATTTTGAGA
<i>IL-10</i>	CAAGGCAGTGGAGCAGGTGAAG	CGCTTTGGTGAGTAGACAGAGGTC
<i>IL-6</i>	TAGTCCTTCTACCCCAATTTCC	TTGGTCCTTAGCCACTCCTTC
<i>CD206</i>	CCTATGAAAATTGGGCTTACGG	CTGACAAATCCAGTTGTTGAGG
<i>iNOS</i>	ATCTTGGAGCGAGTTGTGGATTGTC	TAGGTGAGGGCTTGGCTGAGTG
<i>GAPDH</i>	GGTTGTCTCCTGCGACTTCA	TGGTCCAGGGTTTCTTACTCC

NLRP3, nucleotide-binding and oligomerization domain-like receptor protein 3; HSP90, heat shock protein 90; GSDMD, gasdermin D; IL, interleukin; TNF-α, tumor necrosis factor α; iNOS, inducible nitric oxide synthase.

collected by *in vitro* centrifugation. The TNF-α (EMC102a, Neobioscience Technology Co., Ltd.), IL-1β (EMC001b, Neobioscience Technology Co., Ltd.) and IL-18 [EK218, Hangzhou Multisciences (Lianke) Biotech Co., Ltd.] levels were measured using respective ELISA kits. According to the manufacturer's instructions, the optical density of the samples was measured at 450 nm (OD₄₅₀) using a TECAN SPARK microplate reader (Tecan Group, Ltd.).

RT-qPCR. Total RNA was extracted from the samples in each group using RNA extraction reagents (Nanjing Novizan Medical Technology Co., Ltd.), following the manufacturer's instructions. RNA was quantified using a spectrophotometer and then reverse transcribed into cDNA using PrimeScript™ RT Master Mix kit (cat. no. RR036A, Takara Biotechnology Co., Ltd.). qPCR was performed using PrimeSTAR® Max DNA Polymerase (Takara Biotechnology Co., Ltd.) on an RT-PCR system (Agilent Technologies, Inc.). The samples were amplified using the following thermocycling conditions: Initial denaturation at 95°C for 30 sec; followed by 40 cycles of denaturation at 95°C for 5 sec, annealing at 55°C for 30 sec and elongation at 72°C for 30 sec; and a final extension at 72°C for 10 min. The relative mRNA expression levels of the target genes were calculated as the fold change of the control using the 2^{-ΔΔC_q} method (25). GAPDH primers, obtained from Sangon Biotech (Shanghai) Co., Ltd., were used as the internal reference. The forward and reverse primers used are listed in Table I.

Analysis of caspase activity *in vivo* and *in vitro*. FLIVO (FAM-FLIVO, cat. no. #980) and FLICA (FAM-FLICA, cat. no. #91) probes were obtained from ImmunoChemistry Technologies, LLC. FAM-FLICA is a kit that includes Hoechst and propidium iodide (PI). These are non-cytotoxic fluorescently-labeled inhibitors of caspases that covalently bind active caspases and can be used to quantify caspase activity *in vivo* and *in vitro* and to detect pyroptosis (26,27).

The FLIVO and FLICA probes were dissolved in 50 μl DMSO and used according to the manufacturer's instructions. To evaluate pyroptosis in living animals, the fluorescent green probe, FLIVO, was injected into the tail vein of the mice (n=18) 24 h after the LPS intervention. The FLIVO reagent was allowed to circulate in the mouse systems for 30 min prior to the analysis (28). The mice were then anesthetized using isoflurane (inhalation concentration: 4-5% for induction and 1-3% for maintenance) and fluorescent images were captured using an IVIS Lumina LT Series III instrument (PE, PerkinElmer, Inc.).

To evaluate pyroptosis *in vitro*, the MH-S cells were plated on 25 mm poly-L-lysine-coated coverslips at 3x10⁵ cells per coverslip and incubated with 10 μg/ml LPS for 4 h at 37°C to induce pyroptosis. The cells were fixed with 4% paraformaldehyde for 15 min at room temperature, labeled with FLICA, and incubated for 60 min at 37°C; Subsequently, the cells were washed, stained with Hoechst stain, and incubated for 5 min at room temperature; Finally, the cells were stained with propidium iodide (PI) for 15 min. Images were acquired using a Zeiss two-photon laser confocal microscope (LSM-NLO880, Zeiss AG; x400 magnification).

Protein extraction. The cell samples and lung tissues were lysed using radioimmunoprecipitation assay lysis buffer (Beijing Solarbio Science & Technology Co., Ltd.) containing a phenylmethanesulfonyl fluoride and protein phosphatase inhibitor mixture (Beijing Solarbio Science & Technology Co., Ltd.). The solution was centrifuged at 14,000 x g at 4°C for 20 min, and proteins in the supernatant were quantified using the NanoDrop 2000c spectrophotometer (Thermo Fisher Scientific, Inc.). Proteins were combined with 5X sodium dodecyl-sulfate polyacrylamide gel electrophoresis (SDS-PAGE) loading buffer containing dithiothreitol (P1040; Beijing Solarbio Science & Technology Co., Ltd.) and boiled for 10 min at 100°C. The mixture was then frozen at -80°C until further use.

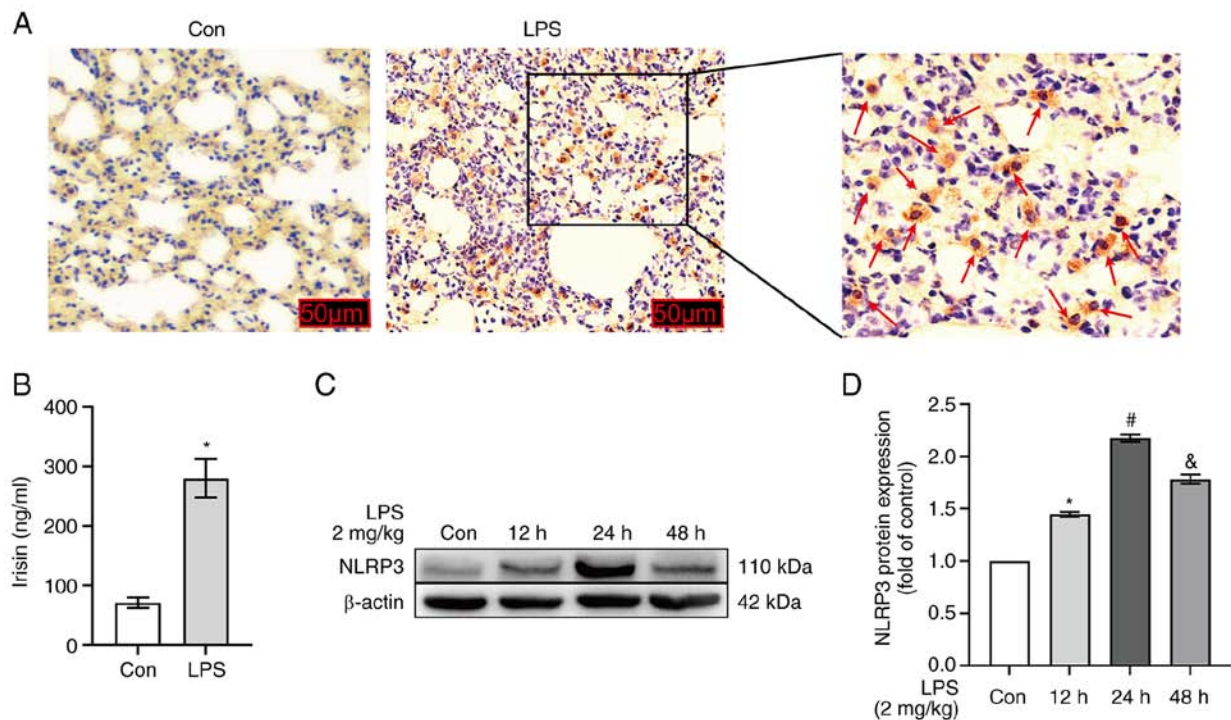


Figure 1. LPS-induced acute lung infection in mice (magnification, x200). (A) FNDC5/irisin was expressed in damaged lung tissue following LPS (2 mg/kg) stimulation. The brown areas shown by the red arrows represent the cytoplasmic expression of FNDC5/irisin. (B) The level of irisin in the serum of mice. (C) The bands of NLRP3 and β -actin obtained using western blotting. (D) Protein expression of NLRP3 at different time periods of LPS (2 mg/kg) stimulation. Data are expressed as the mean \pm standard deviation, n=6. *P<0.05 vs. Con group; #P<0.05 vs. 12 h group; &P<0.05 vs. 24 h group. LPS, lipopolysaccharide; Con, control; NLRP3, nucleotide-binding and oligomerization domain-like receptor protein 3; FNDC5, fibronectin type III repeat-containing protein.

Western blot analysis. Equal quantities of protein (40 μ g/lane) were separated electrophoretically using SDS-PAGE (10-12% gels) and then transferred onto polyvinylidene fluoride membranes (MerckMillipore ISEQ00010, Merck KGaA). The membranes were blocked for 30 min at 25°C with QuickBlock blocking solution (Beyotime Institute of Biotechnology). Subsequently, the membranes were incubated overnight at 4°C with primary antibodies (diluted 1:1,000 in QuickBlock™ Primary Antibody Dilution Buffer, Beyotime Institute of Biotechnology) and then with horseradish peroxidase-conjugated secondary antibodies (diluted 1:10,000 in Tris-buffered saline and Tween-20) for 2 h at 25°C. The expression levels of the target proteins were normalized to those of β -actin, which was used as an internal control. Images were digitally acquired using Amersham Imager 600 (GE Healthcare; Cytiva) chemiluminescence image analysis system. The protein concentration was determined using ImageJ 1.8.0 software (National Institutes of Health).

The primary antibodies used for western blotting were as follows: NLRP3 (cat. no. D4D8T), pro-caspase-1 (cat. no. E2Z1C), cleaved caspase-1 (cat. no. Asp296), IL-1 β (cat. no. 3A6) were purchased from Cell Signaling Technology, Inc.; GSDMD (cat. no. AF4012) was purchased from Affinity Biosciences; HSP90 (cat. no. A5027) was purchased from ABclonal Biotech Co., Ltd.; β -actin (cat. no. 20536-1-AP) was purchased from Proteintech Group, Inc. Secondary antibodies used for western blotting were obtained from the Beyotime Institute of Biotechnology, (HRP-conjugated goat anti-rabbit IgG, cat. no. ZA0277; HRP-conjugated goat anti-mouse IgG, cat. no. A0286), diluted at a ratio of 1:10,000.

Statistical analysis. All experiments were performed at least thrice. Statistical analyses were performed using GraphPad Prism 9 software (GraphPad Software, Inc.). The results are expressed as the mean \pm standard deviation (SD). Bartlett's test was performed to test the homogeneity of variance. The Student's unpaired t-test was used to compare the means of two independent samples. One-way analysis of variance (ANOVA) was performed to compare the differences among groups, and Tukey's post hoc test was used to compare the differences between the two groups following ANOVA. P-values <0.05 were considered to indicate statistically significant differences.

Results

Irisin protects against LPS-induced ALI in mice. Immunohistochemical analysis revealed that FNDC5/irisin was expressed in the damaged lung tissue, but not in normal lung tissue following LPS stimulation (2 mg/kg; Fig. 1A). At the same time, the serum irisin content in mice was detected using an ELISA test kit. The results revealed that LPS significantly increased the serum irisin content in the mice (P<0.05; Fig. 1B). It was hypothesized that the expression of FNDC5/irisin may be driven by the inflammatory responses in the lung tissues. Therefore, the protein expression of NLRP3 was examined at different time periods following LPS stimulation to determine the optimal intervention time. The expression of NLRP3 increased after LPS intervention for 12 and 48 h. However, NLRP3 expression was more significantly upregulated after 24 h of LPS stimulation (2 mg/kg; P<0.05; Fig. 1C and D).

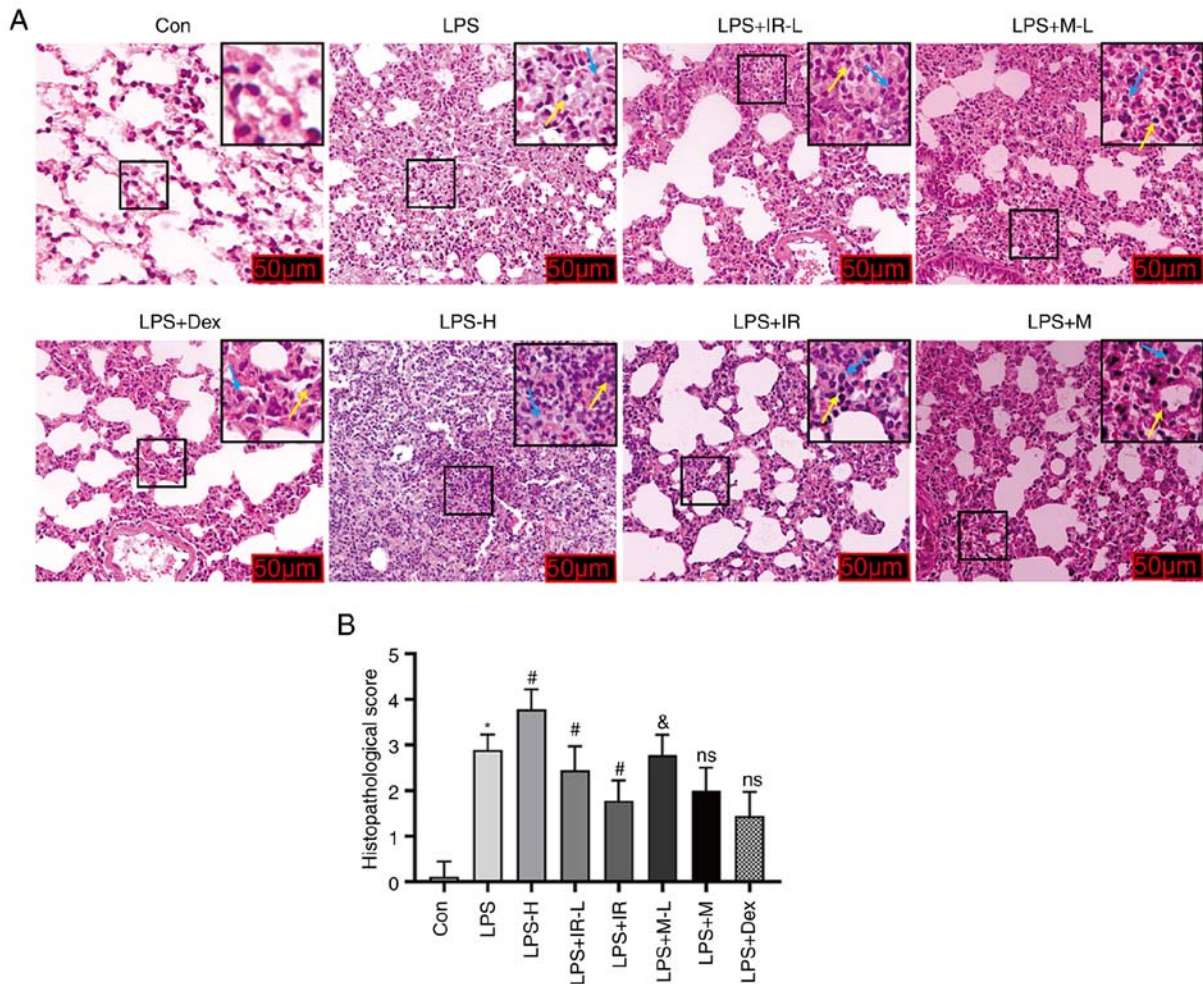


Figure 2. Irisin protects against LPS-induced ALI in mice (magnification, x200). C57BL/6J mice (weighing 18–22 g) aged 6–8 weeks, were randomly assigned to the Con, LPS (LPS 2 mg/kg), LPS-H (LPS 4 mg/kg), LPS + IR-L (LPS 2 mg/kg, irisin 0.25 mg/kg), LPS + IR (LPS 2 mg/kg, irisin 0.5 mg/kg), LPS + M-L (LPS 2 mg/kg, MCC950 25 mg/kg), LPS + M (LPS 2 mg/kg, MCC950 50 mg/kg), and LPS + Dex (LPS 2 mg/kg, dexamethasone 0.5 mg/kg) groups. (A) Lung tissue samples stained with hematoxylin and eosin after 24 h of LPS treatment. Yellow and blue arrows indicate the infiltration of inflammatory cells (lymphocyte and macrophage). (B) The pathological damage scoring of ALI. The data are expressed as the mean \pm SD, $n=6$. * $P<0.05$ vs. Con group; # $P<0.05$ vs. LPS group; & $P<0.05$ vs. LPS + IR group; ns, not significant vs. LPS + IR group. LPS, lipopolysaccharide; ALI, acute lung injury; Con, control.

To verify the anti-inflammatory effects of irisin in animal models of ALI, the indicators of inflammatory damage were examined in mice treated with various drugs. Stimulation with LPS alone significantly damaged the lung tissue through inflammatory cell infiltration, pulmonary interstitial hemorrhage and edema, alveolar wall thickening and diffused alveolar injury compared with the control group. These changes were more evident in the LPS-H (4 mg/kg) stimulation group than those in the LPS (2 mg/kg) group ($P<0.05$; Fig. 2). Exogenous irisin treatment at 0.25 mg/kg effectively alleviated these inflammatory reactions, reduced lung tissue damage and considerably decreased the infiltration of inflammatory cells. However, irisin treatment at 0.5 mg/kg had significant effects compared to the LPS group ($P<0.05$; Fig. 2). It has been confirmed that MCC950 (50 mg/kg) can effectively inhibit LPS-induced neutrophil infiltration in the lungs of mice, identical to Dex (0.5 mg/kg) (29). The present study also demonstrated that high-dose irisin reduced lung inflammation similar to Dex (0.5 mg/kg) and MCC950 (50 mg/kg) ($P>0.05$, Fig. 2B).

Subsequently, the BALF of mice was analyzed to confirm the suppressive effects of irisin on the LPS-induced

inflammatory response. The total number of cells, protein concentrations and neutrophil numbers in BALF in the LPS (2 mg/kg) group increased considerably compared with the control group ($P<0.05$; Fig. 3A–C), but decreased markedly in the LPS + IR group or LPS + MCC950 group. The quantitative data revealed that irisin (0.5 mg/kg) exerted an anti-inflammatory effect equivalent to that of MCC950 (50 mg/kg) (Fig. 3A–C).

NLRP3 is often used as an essential indicator of the inflammatory response. In contrast to the control group, the mRNA and protein expression levels of NLRP3 in mice exposed to LPS were significantly increased ($P<0.05$; Fig. 3D and E), and this increase was considerably reduced by irisin pre-treatment ($P<0.05$; Fig. 3D and E). HSP90 is a molecular chaperone of NLRP3 that plays an essential role in inflammasome assembly and stability. *In vivo*, the expression of HSP90 was upregulated by LPS treatment, while irisin exerted the opposite effect, and MCC950 had no regulatory effect on HSP90 ($P>0.05$; Fig. 3F). Based on this result, it was hypothesized that the mechanism through which irisin attenuates inflammatory lung injury in mice differs from that of MCC950. To examine this

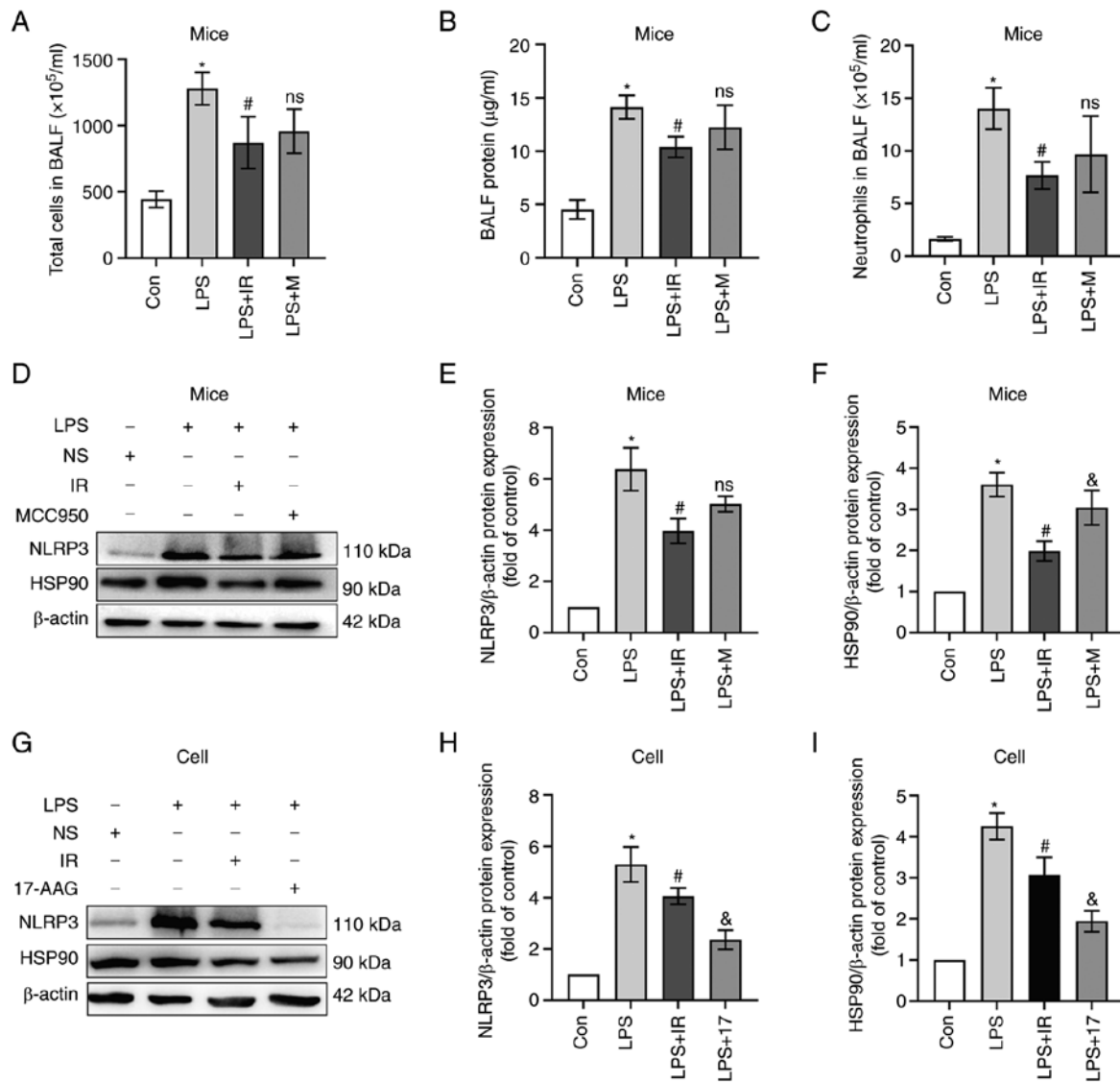


Figure 3. Irisin attenuates the LPS-induced inflammatory response. Mice were randomly assigned to the control, LPS (2 mg/kg), LPS + IR (LPS 2 mg/kg, irisin 0.5 mg/kg), and LPS + MCC950 (LPS 2 mg/kg, MCC950 50 mg/kg) groups (n=6). MH-S cells (n=3) were co-treated with IR (200 ng/ml) or 17-AAG (100 ng/ml) and LPS (10 $\mu\text{g}/\text{ml}$) for 4 h. Western blotting was used to measure NLRP3 and HSP90 protein expression. (A) Total number of cells, (B) proteins, and (C) neutrophils in the specimens of BALF. (D-I) Irisin inhibited the activation of the NLRP3 inflammasome and the expression of HSP90 in mice and MH-S cells. The data are expressed as the mean \pm SD. *P<0.05 vs. Con group; #P<0.05 vs. LPS group; &P<0.05 vs. LPS + IR group; ns, not significant vs. LPS + IR group. LPS, lipopolysaccharide; BALF, bronchoalveolar lavage fluid; Con, control; NLRP3, nucleotide-binding and oligomerization domain-like receptor protein 3; HSP90, heat shock protein 90; 17-AAG, 17-N-allylamino-17-demethoxygeldanamycin.

hypothesis and elucidate the underlying mechanisms of the anti-inflammatory effect of irisin, an *in vitro* experiment was performed using 17-AAG (an inhibitor of HSP90)-treated cells as the positive control (Fig. 3G-I). It was found irisin exerted a similar effect to that of 17-AGG in reducing inflammasome production.

Irisin protects against LPS-induced cell damage. CCK-8 assays were used to determine the effects of various concentrations of LPS, irisin and 17-AAG on cell viability. LPS stimulation at 100 $\mu\text{g}/\text{ml}$ for 24 h decreased cell viability (P<0.05; Fig. 4A), while LPS stimulation at 10 $\mu\text{g}/\text{ml}$ for 4 h did not affect cell viability (P>0.05; Fig. 4B). Therefore, 10 $\mu\text{g}/\text{ml}$ LPS was used in subsequent experiments. Irisin at <400 ng/ml had no significant toxic effects on the MH-S cells (P>0.05; Fig. 4C). The cell numbers decreased with the increasing concentrations of

17-AAG, and 100 ng/ml was selected as the final concentration for the intervention (P>.05; Fig. 4D). The intervention of MH-S cells with LPS for different periods of time revealed that LPS (10 $\mu\text{g}/\text{ml}$) stimulation significantly upregulated NLRP3 expression in the cells treated for 4 h compared to those in the untreated cells or the cells treated for 2 h (P<0.05; Fig. 4E and F).

Irisin inhibits the release of pro-inflammatory cytokines by regulating the polarization of AMs. To evaluate the inhibitory effects of irisin on the release of pro-inflammatory cytokines *in vivo* and *in vitro*, ELISA kits were used to detect IL-1 β , IL-18 and TNF- α secretion in the BALF and serum of mice and MH-S cell culture supernatants. The results revealed that the IL-1 β , IL-18 and TNF- α levels significantly increased in the LPS group compared with the control group (P<0.05; Fig. 5).

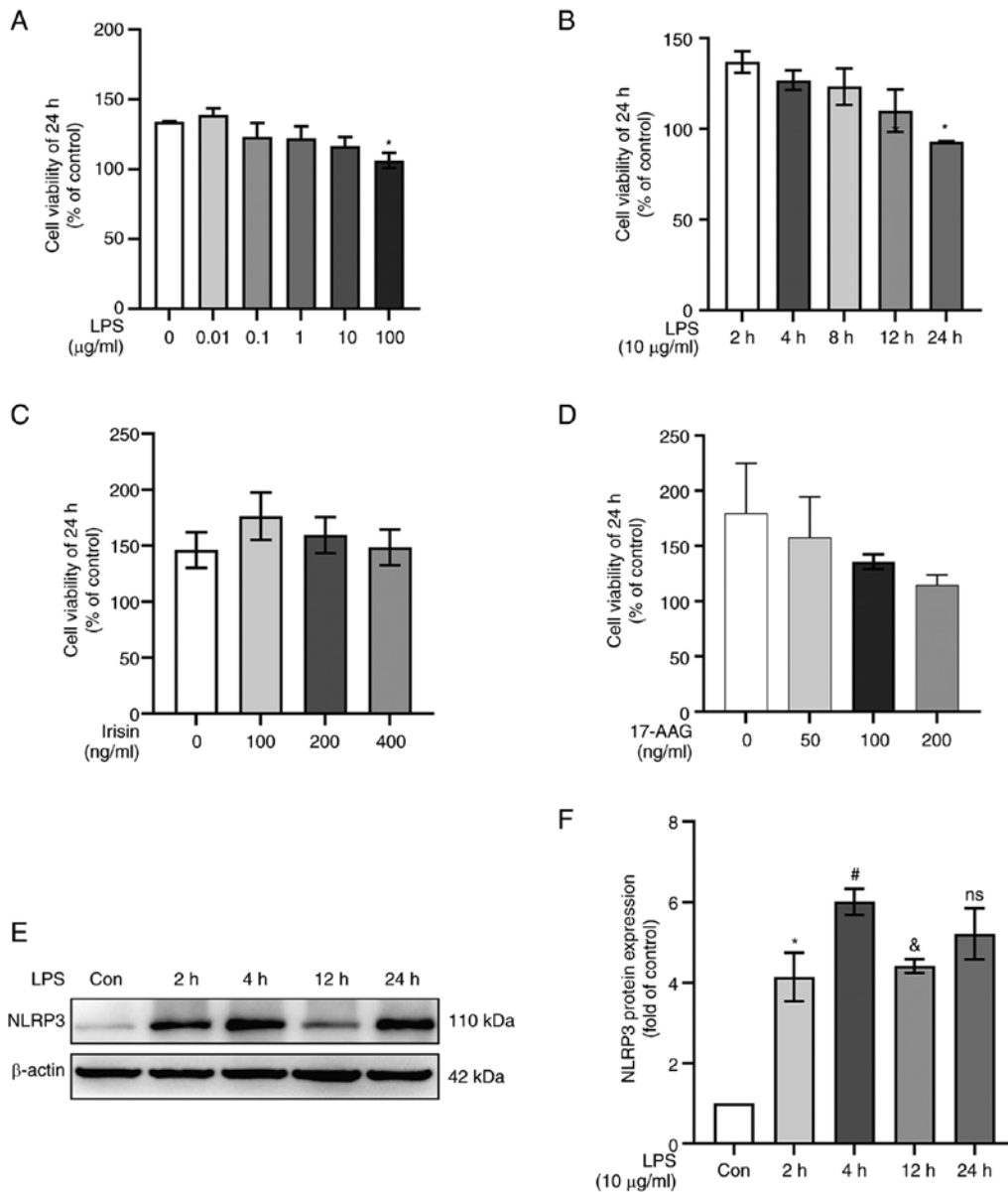


Figure 4. Irisin protects against LPS-induced cell damage. The data are expressed as mean \pm SD, $n=3$. (A) MH-S cells were treated with various concentrations (0, 0.01, 0.1, 1, 10 and 100 $\mu\text{g/ml}$) of LPS for 24 h and analyzed using CCK-8 assay. * $P<0.05$ vs. 0 $\mu\text{g/ml}$ group. (B) CCK-8 assay results of LPS (10 $\mu\text{g/ml}$)-treated MH-S cells measured at different time points. * $P<0.05$ vs. 2 h group. (C and D) CCK-8 assay to detect the cytotoxicity of irisin (0, 100, 200 and 400 ng/ml) and 17-AAG (0, 50, 100 and 200 ng/ml) in MH-S cells. (E and F) Quantitative analysis of NLRP3 protein expression at different time points of LPS stimulation (10 $\mu\text{g/ml}$). * $P<0.05$ vs. Con group; # $P<0.05$ vs. 2 h group; & $P<0.05$ vs. 4 h group; ns, not significant vs. 4 h group. LPS, lipopolysaccharide; Con, control; 17-AAG, 17-N-allylamino-17-demethoxygeldanamycin.

Compared with the LPS group, irisin effectively decreased the IL-1 β and IL-18 levels in BALF ($P<0.05$; Fig. 5A and B), serum ($P<0.05$, Fig. 5A and B) and cell culture supernatants ($P<0.05$ Fig. 5A and B). MCC950 also had similar suppressive effects on the levels of IL-1 β and IL-18 in BALF ($P<0.05$, Fig. 5A and B), serum ($P<0.05$, Fig. 5A and B). On the contrary, irisin effectively suppressed the release of TNF- α ($P<0.05$, Fig. 5C), while MCC950 did not (Fig. 5C). *In vitro*, 17-AAG considerably reduced the LPS-induced release of IL-1 β and IL-18 ($P<0.05$ Fig. 5A and B), and slightly decreased the levels of TNF- α ($P<0.05$, Fig. 5C).

RT-qPCR was used to detect the mRNA expression of inflammatory factors in mice and MH-S cells. The results revealed that compared with the control group, LPS significantly induced the release of IL-1 β , IL-18 and TNF- α in lung

tissue and MH-S cells ($P<0.05$, Fig. 6). Compared with the LPS group, irisin reduced the release of IL-1 β ($P<0.05$, Fig. 6A), IL-18 ($P<0.05$, Fig. 6B) and TNF- α ($P<0.05$, Fig. 6C) in the lung tissue. The mRNA levels of these inflammatory factors were also reduced *in vitro* ($P<0.05$, Fig. 6D-F) in the irisin-treated cells compared with those in the LPS-stimulated cells. Furthermore, the mRNA expression of IL-1 β ($P<0.05$, Fig. 6A) and IL-18 ($P<0.05$, Fig. 6B) in the MCC950-treated mice was lower compared with that in the LPS-exposed mice; however, no marked inhibitory effect of MCC950 was observed on TNF- α levels compared with the LPS group ($P>0.05$, Fig. 6C). The suppressive effects of 17-AAG on IL-1 β ($P<0.05$, Fig. 6D) and IL-18 ($P<0.05$ Fig. 6E) levels were similar to those of irisin; however, the suppressive effects of irisin on TNF- α levels were more prominent than those of 17-AAG ($P<0.05$, Fig. 6F).

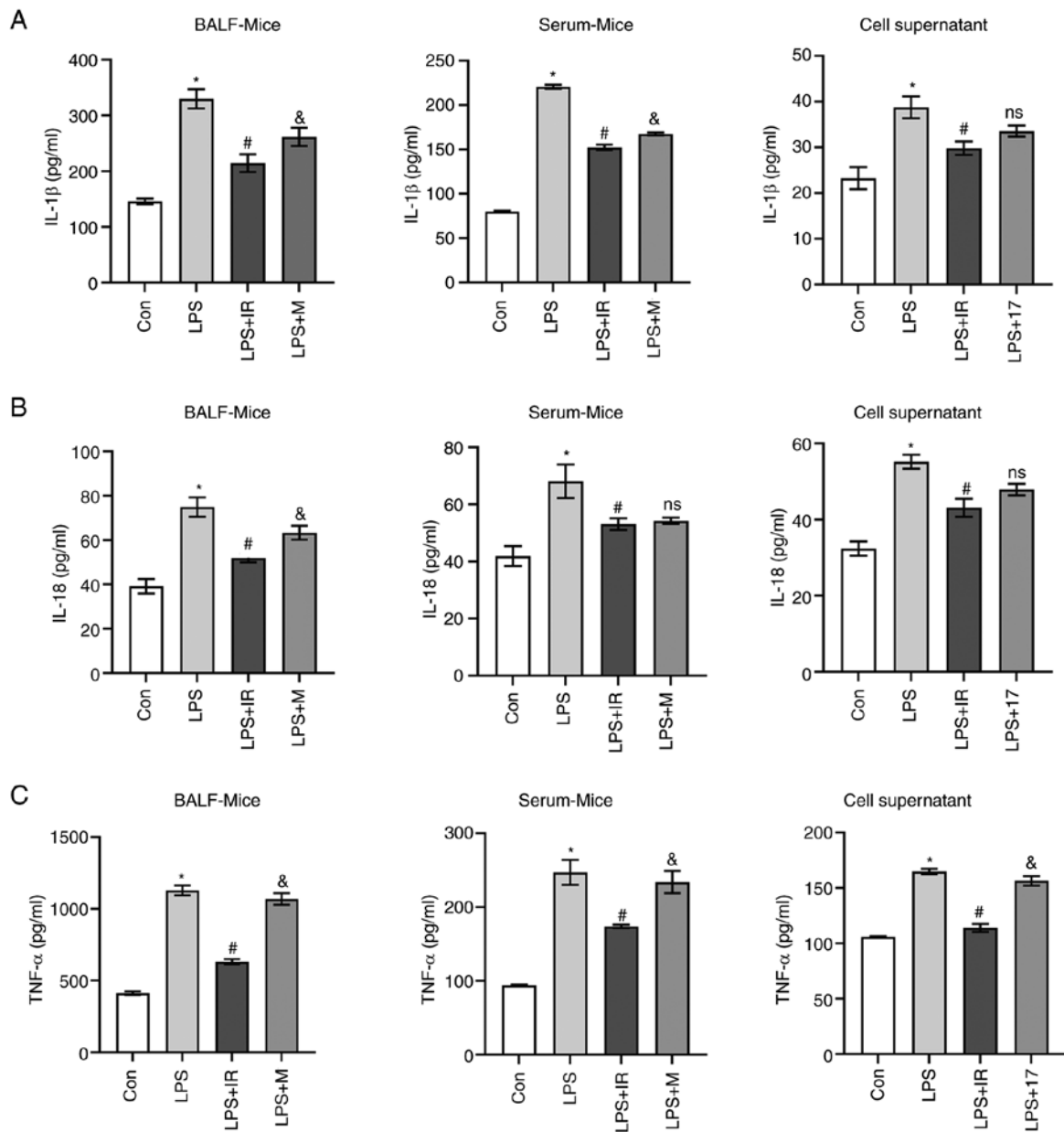


Figure 5. Irisin inhibits the release of pro-inflammatory cytokines. Mice were randomly assigned to the control, LPS (2 mg/kg), LPS + IR (LPS 2 mg/kg, irisin 0.5 mg/kg), and LPS + MCC950 (LPS 2 mg/kg, MCC950 50 mg/kg) groups (n=6). Following treatment, serum and BALF samples were collected. MH-S cells were co-cultured with LPS (10 μ g/ml) and IR (200 ng/ml) or 17-AAG (100 ng/ml) for 4 h (n=3). ELISA was used to detect IL-1 β , IL-18, and TNF- α secretion in (A) BALF, (B) serum, and (C) cell supernatant samples. The data are expressed as the mean \pm SD. *P<0.05 vs. Con group; #P<0.05 vs. LPS group; &P<0.05 vs. LPS + IR group; ns, not significant vs. LPS + IR group. LPS, lipopolysaccharide; Con, control; 17-AAG, 17-N-allylamino-17-demethoxygeldanamycin; IL, interleukin; TNF- α , tumor necrosis factor α .

Subsequently, iNOS and CD206 antibodies were used as biomarkers for AMs to evaluate macrophage polarization *in vivo* and *in vitro*. Immunofluorescence co-staining with CD68 and iNOS confirmed that LPS promoted the transformation of AMs to the M1 type *in vivo* and *in vitro* (iNOS, P<0.05; Fig. 7E and G) compared with the control group. Irisin pre-treatment increased the numbers of M2 macrophages compared with the LPS group (CD206, P<0.05; Fig. 7F and H). This may be due to a significantly increased co-localization and reduced differentiation of macrophages to the M1 type (iNOS, P<0.05; Fig. 7B, E and G). Compared with irisin, LPS, MCC950 and 17-AAG had a lesser effect on the regulation of M2-type macrophages (Fig. 7).

The visualization of cell morphology using Operetta CLS revealed that the MH-S cells in the control group had an oval shape with complete cell membranes (30). Cell morphology tracking technology revealed that numerous cells had irregular shapes, increased protrusions, longer pseudopodia, cell swelling or vesicle-like changes and ruptured cell membranes following LPS (10 μ g/ml) stimulation. Irisin protected the cells from morphological changes, whereas 17-AAG did not (Fig. 8A). The results of RT-qPCR revealed that the mRNA expression levels of the M1 macrophage biomarkers, iNOS and IL-6, *in vivo* and *in vitro* were significantly higher in the LPS group than in the control group (P<0.05; Fig. 8B and D). Compared with the Con group, LPS increased the levels of

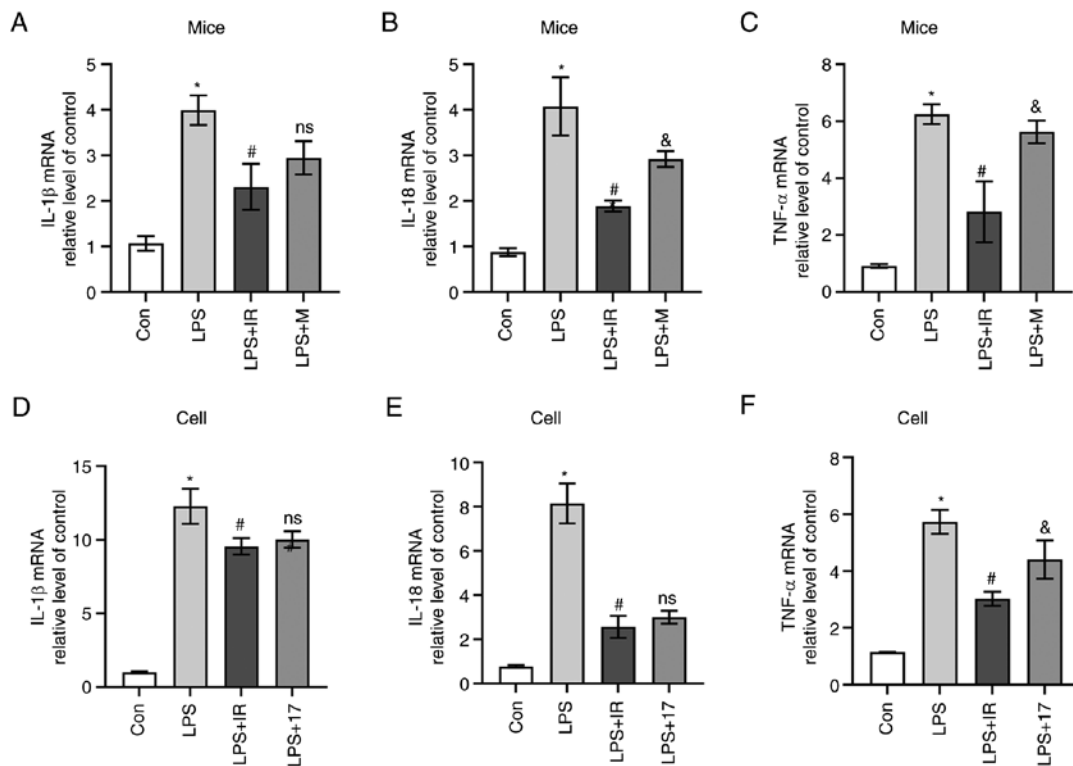


Figure 6. Irisin inhibits the mRNA expression of pro-inflammatory cytokines. The grouping of mice and cells is the same as that in Fig. 5. Reverse transcription-quantitative PCR was used to detect the mRNA expression of IL-1 β , IL-18 and TNF- α in (A-C) lung tissues and (D-F) MH-S cells. The data are expressed as the mean \pm SD. * P <0.05 vs. Con group; # P <0.05 vs. LPS group; [&] P <0.05 vs. LPS + IR group; ns, not significant vs. LPS + IR group. LPS, lipopolysaccharide; Con, control; M, MCC950; IR, irisin; 17, 17-AAG (17-N-allylamino-17-demethoxygeldanamycin).

the M2 macrophage biomarkers, CD206 and IL-10, in mouse lung tissue and cells (P <0.05; Fig. 8C and E). Macrophages can self-regulate the phenotype, which may be due to the polarization of macrophages themselves to LPS-induced inflammatory responses. Irisin reversed the elevated expression of iNOS and IL-6 induced by LPS, promoting the high expression of CD206 and IL-10 *in vivo* and *in vitro* (P <0.05; Fig. 8B-E).

Irisin inhibits macrophage pyroptosis. The destroyed integrity of the cell membrane characterizes pyroptosis. Pyroptotic cells exhibit swelling, and numerous bubble-like protrusions appear on the surface of the cellular membrane before its rupture. Still, DNA damage and chromatin condensation occur after the break of the cell membrane (31). It has been found that pyroptotic cells are permeable to 7-AAD and PI due to the low weight of these dyes (32). The present study used the Calcein AM/7-AAD double staining method to distinguish living cells from cells with damaged membranes. When pyroptosis occurs in cells, the cell membranes are damaged and do not have cell activity, and thus they can be stained red. Some cells in the early stages of pyroptosis can be double-stained by Calcein AM and 7-AAD, and the cells are stained green and red simultaneously. As shown in Fig. 9A, the majority of the cells in the LPS group were colored red, proving that the cell membrane was damaged, and pyroptosis had occurred. The number of red-stained cells in the irisin and 17-AAG groups was relatively reduced, demonstrating that the number of pyroptotic cells was decreased.

Immunofluorescence experiments were also performed using the M1 macrophage-specific antibody, CD80 (green

fluorescence), and the pyroptotic executive protein antibody, GSDMD (red fluorescence). More green fluorescent particles were located in M1 macrophages specifically labeled with CD80 antibody (Fig. 9D and E). The results revealed that *in vivo* and *in vitro*, M1 macrophages (green fluorescence) in the LPS group were stained red by the GSDMD antibody. Compared with LPS, irisin reduced the occurrence of pyroptosis (P <0.05; Fig. 9B and C). Therefore, it was deemed that M1 macrophages undergo pyroptosis.

Irisin inhibits caspase-1 activity. The production of IL-1 β and IL-18 is associated with pyroptosis, and caspase-1 is a core factor in the initiation of pyroptosis (14). The present study used FLIVO to detect caspase-1 enzyme activity in mice. LPS significantly enhanced the fluorescence of caspase-1, which was evenly distributed in multiple lung lobes and was substantially more potent than that in the control group (P <0.05; Fig. 10A and B). Compared with the LPS group, fewer FLIVO fluorophores and a lower fluorescence intensity in the lung lobes of mice were observed in the irisin group, confirming that irisin reduced caspase-1 activity (P <0.05; Fig. 10A and B). The results of the immunofluorescence staining of frozen sections of mouse lung tissue were consistent with the results of the *in vivo* experiments, confirming that irisin inhibited the activity of caspase-1 in mice (P <0.05; Fig. 10C and D). The results of the *in vivo* experiments revealed that MCC950 did not play a role in inhibiting the activity of caspase-1 (Fig. 10C and D).

For the *in vitro* experiments, FLICA was selected as the detection reagent for the intracellular activity of the caspase-1 enzyme. At the same time, the PI staining of the cells with

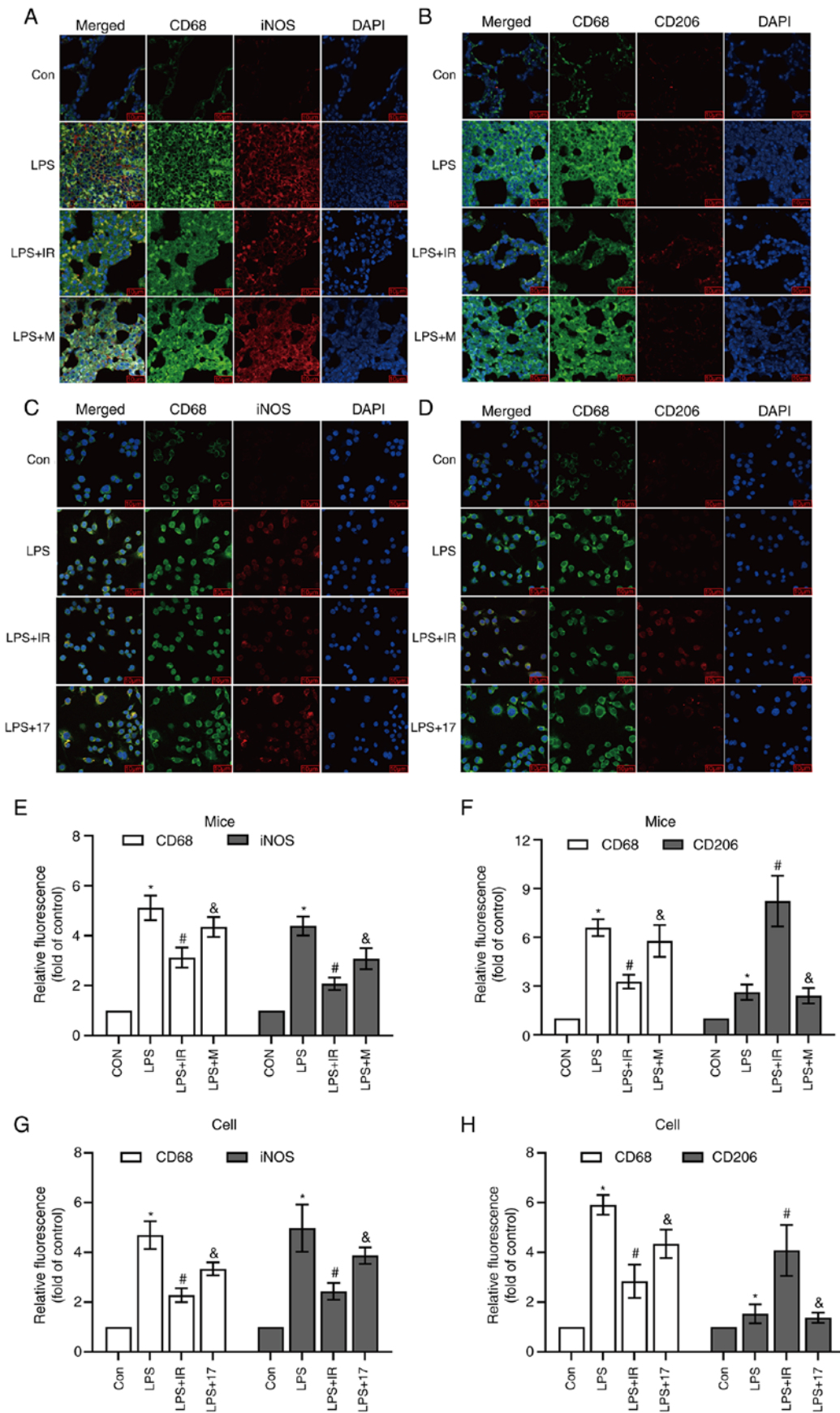


Figure 7. Irisin regulates alveolar macrophage polarization *in vivo* and *in vitro*. The experimental groupings are as those described in Fig. 5. Immunofluorescence co-staining with CD68 and the M1-type macrophage biomarker, iNOS, or the M2-type macrophage biomarker, CD206. Blue color indicates DAPI staining; green color indicates CD68 staining; red color indicates iNOS or CD206 staining. Merged figures show the overlap. (A and B) Immunofluorescence of macrophage typing in mouse lung tissue. (C and D) Immunofluorescence of cell samples. (E-H) Quantitative analysis of fluorescence intensity using ImageJ software. The data are expressed as the mean \pm SD. * $P < 0.05$ vs. Con group; # $P < 0.05$ vs. LPS group; & $P < 0.05$ vs. LPS + IR group. LPS, lipopolysaccharide; Con, control; M, MCC950; IR, irisin; 17, 17-AAG (17-N-allylamino-17-demethoxygeldanamycin); iNOS, inducible nitric oxide synthase.

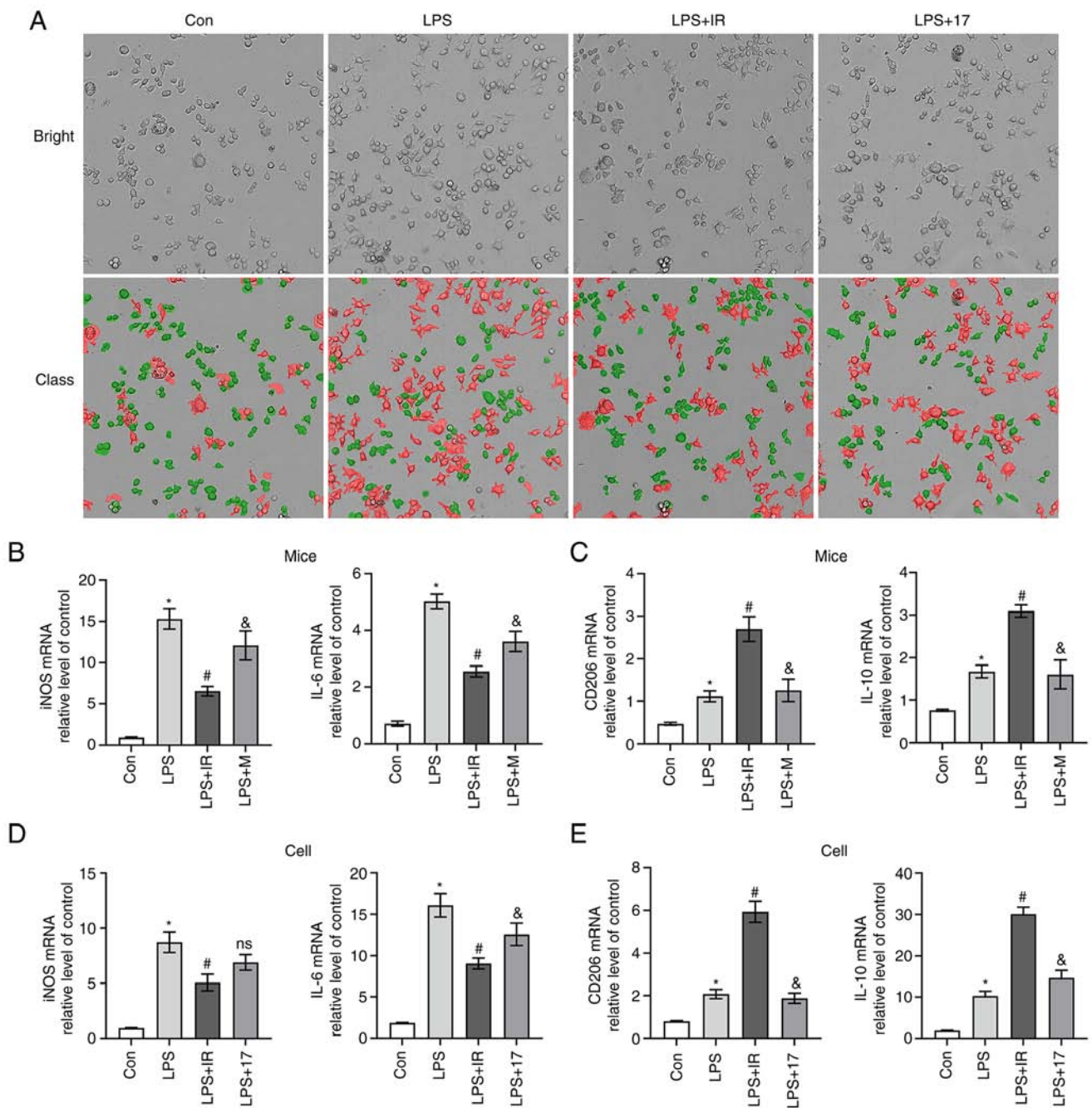


Figure 8. Irisin regulates macrophage polarization. (A) Cell morphology analyzed using Perkin Elmer Operetta CLS. (B-E) mRNA expression of M1-type biomarkers (iNOS and IL-6) and M2-type biomarkers (CD206 and IL-10) in mice (n=6) and MH-S cells (n=3) quantified using RT-qPCR. The data are expressed as the mean \pm SD. *P<0.05 vs. Con group; #P<0.05 vs. LPS group; &P<0.05 vs. LPS + IR group; ns, not significant vs. LPS + IR group. LPS, lipopolysaccharide; Con, control; M, MCC950; IR, irisin; 17, 17-AAG (17-N-allylamino-17-demethoxygeldanamycin); iNOS, inducible nitric oxide synthase.

damaged membranes confirmed that cells at an early stage of pyroptosis (stained in both green and red) had damaged membranes, but were not completely dead. The results of immunofluorescence confocal staining revealed that the activity of caspase-1 in the LPS group was significantly higher than that in the control group (P<0.05; Fig. 10E and F). Irisin effectively reduced the LPS-induced activation of caspase-1 (P<0.05; Fig. 10E and F). 17-AAG exerted a similar effect as irisin (P>0.05 vs. irisin group; Fig. 10E and F). As shown in Fig. 10E (reds arrow), in the cells double-stained with FLICA and PI, the integrity of the cell membrane was disrupted, suggesting that the cell was undergoing pyroptosis (32).

Irisin inhibits caspase-1-mediated pyroptosis by regulating the HSP90/NLRP3 signaling pathway. LPS significantly increased the expression and release of HSP90, NLRP3 and increased caspase-1 in mice, while upregulating the GSDMD and IL-1 β levels (P<0.05 Fig. 11A and C-H). Similar results were observed when the MH-S cells were analyzed (P<0.05 Fig. 11B and I-N). This confirmed that the LPS-induced pyroptosis of murine AMs amplifies the inflammatory response. The results of western blot analysis (Fig. 11) and RT-qPCR (Fig. 12) revealed that irisin significantly inhibited the LPS-induced overexpression of HSP90 and NLRP3. It also reduced pro-caspase-1 activity and decreased the expression

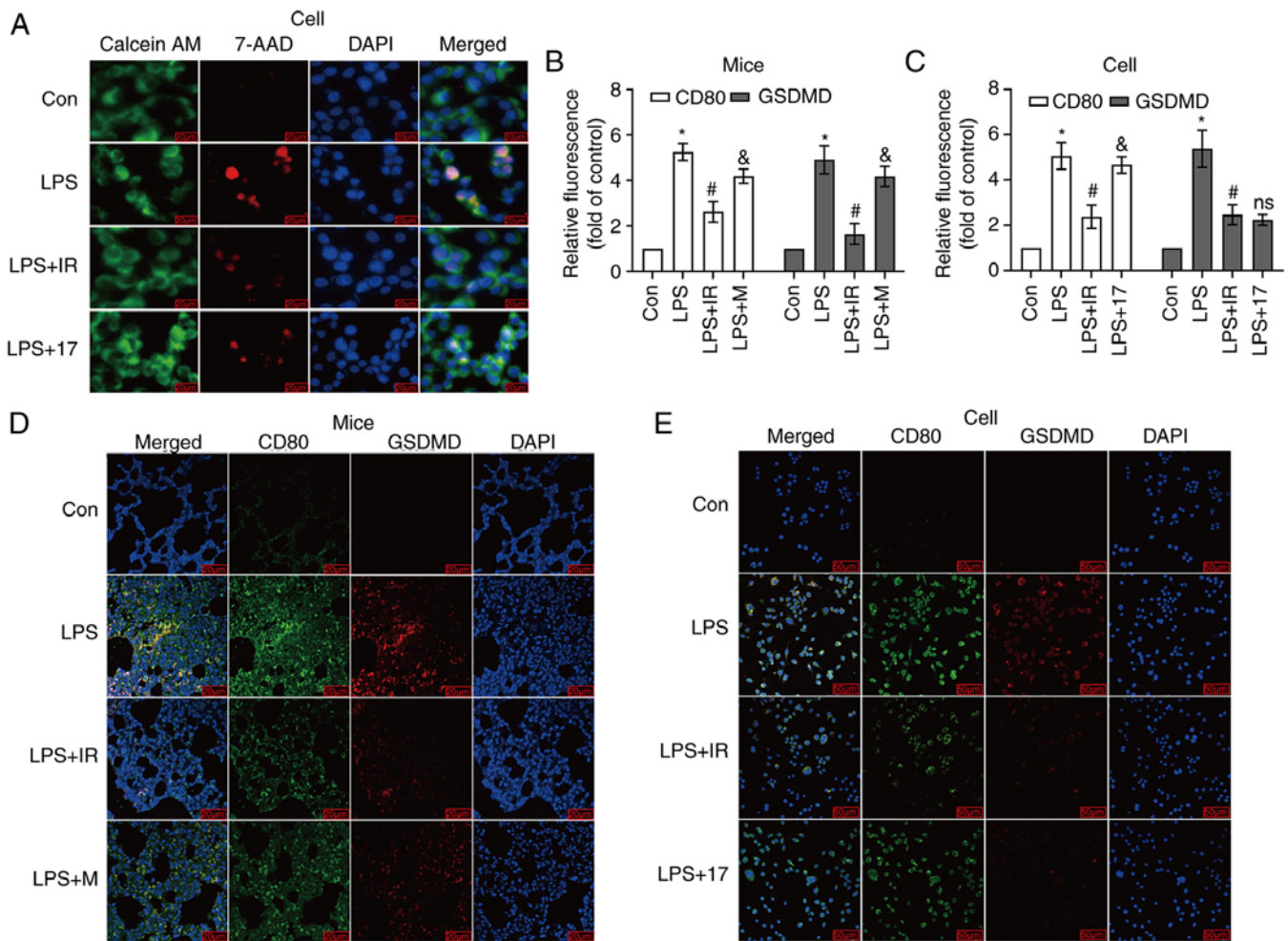


Figure 9. (A) Calcein AM/7-AAD double staining detected pyroptosis (n=3, magnification, x400). Blue color indicates DAPI staining; green color indicates Calcein AM staining; red color indicates 7-AAD staining. The cells stained in green and red represent ongoing pyroptosis. The experimental groupings are as those described in Fig. 5. (B and C) Quantitative analysis of fluorescence intensity using ImageJ software. (D and E) Immunofluorescence co-staining with the M1-type macrophage biomarker, CD80, and pyroptotic executive protein antibody (GSDMD) in mice (n=6, magnification, x400) and MH-S cell (n=3, magnification, x200). Blue color indicates DAPI staining; green color indicates CD80 staining; red color indicates GSDMD staining. The data are expressed as the mean \pm SD. *P<0.05 vs. Con group; #P<0.05 vs. LPS group; &P<0.05 vs. LPS + IR group; ns, not significant vs. LPS + IR group. LPS, lipopolysaccharide; Con, control; M, MCC950; IR, irisin; 17, 17-AAG (17-N-allylamino-17-demethoxygeldanamycin); iNOS, inducible nitric oxide synthase; GSDMD, gasdermin D.

of cleaved caspase-1, GSDMD and IL-1 β , indicating the inhibition of pyroptosis.

As shown in Figs. 11 and 12, *in vivo*, MCC950 reduced the expression of cleaved caspase-1 but had no noticeable inhibitory effect on the overexpression of GSDMD. *In vitro*, 17-AAG inhibited the levels of HSP90 and NLRP3, and decreased GSDMD expression. Irisin played a role similar to that of 17-AAG, confirming that irisin can regulate the HSP90/NLRP3 signaling pathway and reduce LPS-induced caspase-1-dependent macrophage pyroptosis.

Discussion

The novel coronavirus disease 2019 (COVID-19) has swept the world since 2019 and is still affecting human health across the globe. One of the major complications of COVID-19, ALI/ARDS, is responsible for the death of patients. A previous study demonstrated that AM death activated multiple signaling pathways upon lung injury and led to the release inflammatory mediators, such as IL-1 β , IL-6, IL-18 and TNF- α (33).

Inflammatory cell infiltration destroys the alveolar epithelium and pulmonary microvascular barrier, accelerates lung inflammation and aggravates lung tissue damage (34). Therefore, regulating AM death may be a potential therapeutic strategy for controlling ALI/ARDS. In the present study, both *in vitro* cell experiments and *in vivo* mouse models were used. It was demonstrated that irisin, a myokine with anti-inflammatory effects that regulate cell signaling pathways, protects against LPS-induced cell damage and ALI in mice. It inhibited the release of pro-inflammatory cytokines by regulating the polarization of AM, AM pyroptosis, and caspase-1-mediated pyroptosis.

Irisin is the product of FNDC5 hydrolysis. Unlike previous studies (19,20), the present study found that FNDC5 was expressed in the lungs of mice with LPS-induced inflammatory injury, and it was hypothesized that irisin may have a positive anti-inflammatory effect. Inflammatory cell infiltration in mouse lung tissue was significantly reduced following treatment with irisin, confirming that irisin can improve LPS-induced ALI. Macrophages are divided into two subgroups: M1 and

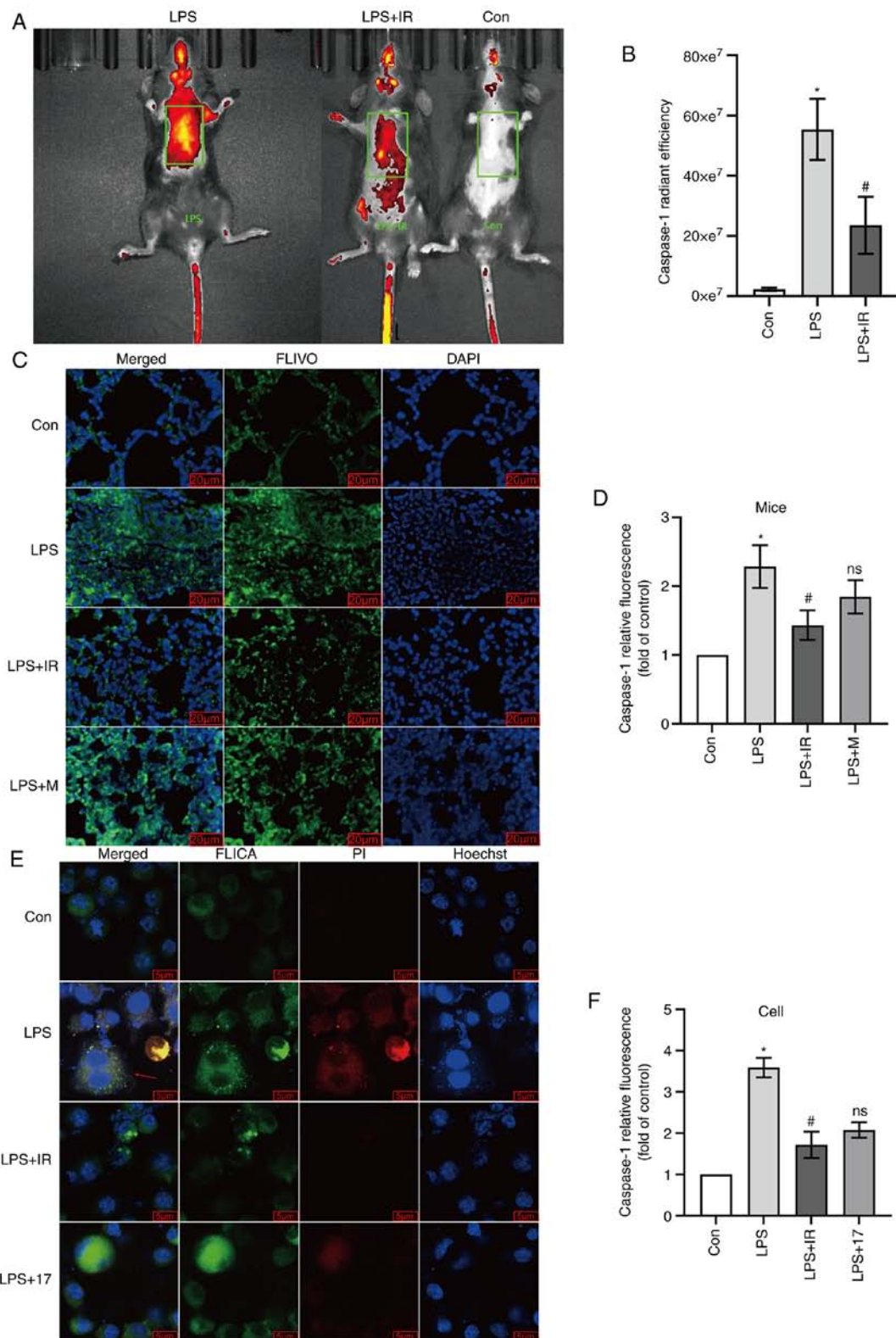


Figure 10. Irisin inhibits caspase-1 activity *in vivo* (n=6) and *in vitro* (n=3). Mice were randomly assigned to the control, LPS (2 mg/kg), and LPS + IR (LPS 2 mg/kg, irisin 0.5 mg/kg) groups. (A) FLIVO detected caspase-1 enzyme activity in mice. (B) Quantitative analysis of *in vivo* staining in mice. (C) The immunofluorescence staining of frozen sections of mouse lung tissue. The merged image represents the overlap of FLIVO- and DAPI-stained sections. Green color indicates FLIVO staining, blue color indicates DAPI staining. (D) Statistical analysis of caspase-1 fluorescence value in mice lung tissue. (E) FLICA detected caspase-1 enzyme activity in cells. (F) Statistical analysis of caspase-1 fluorescence value *in vivo*. The data are expressed as the mean \pm SD. *P<0.05 vs. Con group; #P<0.05 vs. LPS group; ns, not significant vs. LPS + IR group. LPS, lipopolysaccharide; Con, control.

M2 (35). M1-type macrophages play a role in inflammatory activation, while M2-type macrophages are involved in the resolution of inflammation (36). In the early stages of ALI,

high levels of pro-inflammatory factors, such as IL-1 β , TNF- α and iNOS in the body induce M1-type macrophages to continuously expand the inflammatory response. Over time, IL-4 and

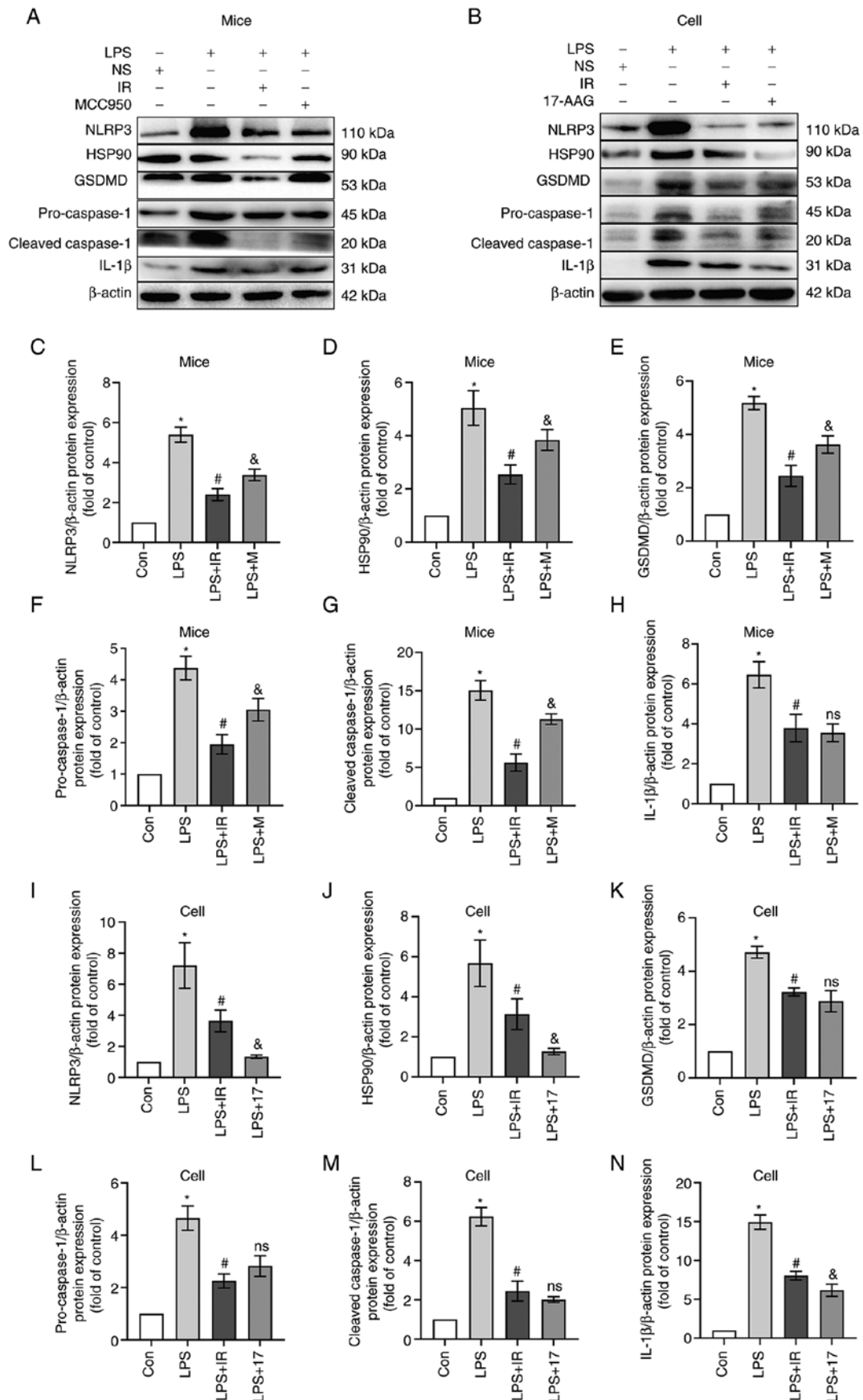


Figure 11. Irisin inhibits caspase-1-mediated pyroptosis by regulating the HSP90/NLRP3 signaling pathway. The grouping of mice and cells is the same as in Fig. 5. (A and B) After drug treatment, proteins were extracted from (A) lung tissue and (B) MH-S cells and subjected to western blotting to determine the expression levels of NLRP3, HSP90, GSDMD, caspase-1, cleaved caspase-1 and IL-1 β proteins. (C-N) Relative quantitative analysis of protein expression. The data are expressed as the mean \pm SD. * P <0.05 vs. Con group; # P <0.05 vs. LPS group; & P <0.05 vs. LPS + IR group; ns, not significant vs. LPS + IR group. LPS, lipopolysaccharide; Con, control; NLRP3, nucleotide-binding and oligomerization domain-like receptor protein 3; HSP90, heat shock protein 90; GSDMD, gasdermin D; IL, interleukin; M, MCC950; IR, irisin; 17, 17-AAG (17-N-allylamino-17-demethoxygeldanamycin).

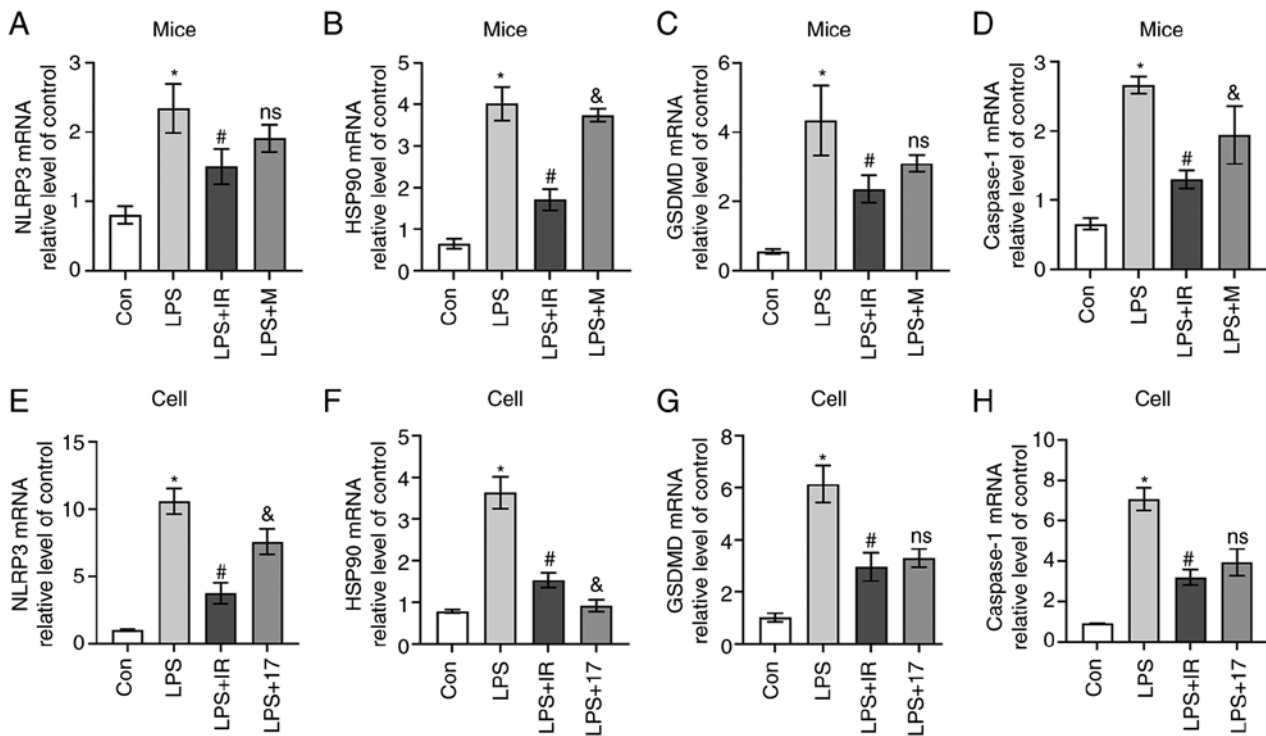


Figure 12. RT-qPCR analysis of (A and E) NLRP3, (B and F) HSP90, (C and G) GSDMD, and (D and H) Caspase-1 mRNA expression *in vivo* (n=6, A-D) and *in vitro* (n=3, E-H). The data are expressed as the mean \pm SD. *P<0.05 vs. Con group; #P<0.05 vs. LPS group; &P<0.05 vs. LPS + IR group; ns, not significant vs. LPS + IR group. LPS, lipopolysaccharide; Con, control; M, MCC950; IR, irisin; 17, 17-AAG (17-N-allylamino-17-demethoxygeldanamycin); GSDMD, gasdermin D; NLRP3, nucleotide-binding and oligomerization domain-like receptor protein 3; HSP90, heat shock protein 90.

IL-13 induce the production of M2-type macrophages. They express and produce the anti-inflammatory factors, IL-10 and IL-1R α , which play a role in tissue damage repair (37). The present study confirmed that irisin pre-treatment significantly increased the transcription and release of CD206 and IL-10 compared to LPS pre-treatment. It reduced IL-1 β , IL-18 and TNF- α expression *in vivo* and *in vitro*, indicating that irisin can regulate the transformation of AMs into the M2 type, and can play a role in inhibiting inflammation and repairing tissue damage.

Pyroptosis is also known as programmed necrotic death. Unlike the apoptotic pathway, the pyroptotic pathway often exhibits features of necrosis and amplifies inflammatory signaling by altering the permeability of the cell membrane to release the cellular contents (38,39). To examine the permeability of the cell membrane, the present study used CalceinAM/7-AAD double staining. Calcein-AM can easily penetrate the membrane of living cells, fluorescently label living cells, and emit uniform green solid fluorescence in living cells. It has the characteristics of low cytotoxicity and can reduce damage to cells. 7-AAD is a non-permeable fluorescent nuclear dye that cannot penetrate the cell membrane of normal living cells, but can penetrate cells with membrane damage and can embed into the DNA of necrotic cells to form highly fluorescent adducts that emit red fluorescence. Therefore, 7-AAD only stains cells with damaged membranes (40). The present study found that the majority of the cells in the LPS group were colored red, proving that the cell membrane is damaged and pyroptosis had occurred. Considering that this experiment is not specific, the present study further applied FLICA dyes in subsequent cell experiments to verify that caspase-1 was

activated and pyroptosis had occurred. The principal steps of pyroptosis involve the activation of caspase-1 mediated via the inflammasome complex to cleave GSDMD, leading to the perforation of the cell membrane followed by cell swelling, rupture and release of cellular contents (41). Caspase-1 cuts pro-IL-1 β or pro-IL-18 to promote the production and release of IL-1 β and IL-18, respectively (42). The staining of live and membrane-damaged cells revealed that LPS induced the pyroptosis of MH-S cells, in which membrane-damaged cells appeared red due to staining with 7-AAD. Simultaneously, ELISA assays revealed that the IL-1 β and IL-18 levels in the culture supernatant of the LPS group were significantly higher than those of the control group, confirming that the MH-S cells had undergone pyroptosis. The present study performed a preliminary exploration of the types of macrophages that undergo pyroptosis. The *in vivo* and *in vitro* immunofluorescence experiments revealed that the majority of the cells labeled by CD80 (specific antibody for M1 macrophages, green fluorescence) in the LPS group were also stained red (GSDMD antibody). Accordingly, it was hypothesized that M1 macrophages undergo pyroptosis under the stimulation of LPS. Irisin reduced the occurrence of pyroptosis.

FLIVO and FLICA were used to bind activated caspase-1 *in vivo* and *in vitro*, after which caspase activity was quantified to detect pyroptosis. The results indicated that irisin reduced caspase-1 activity and pyroptosis *in vivo* and *in vitro*. NLRP3 is the promoter of pyroptosis. It was found that NLRP3 was intuitively increased with the number of dead cells. It was hypothesized that it could be explained by the following reasons: i) Dead cells release more NLRP3, indicating that other pathways may promote the expression of NLRP3; ii) following

LPS intervention, a specific reaction against pyroptosis occurred in the cells, which caused the reduction of NLRP3 in the cells at 12 h of LPS intervention. Luo *et al* (43) found that the expression of NLRP3 was upregulated in NR8383AM cells exposed to LPS at 6 h; the presentation of NLRP3 was decreased at 12 h of LPS intervention. The mRNA of NLRP3 was increased when exposed to LPS for 24 h compared with that at 12 h (43). The results of the present study were similar to these. The expression of NLRP3 was increased following LPS intervention in the MH-S cells at 4 h, but was reduced at 12 h. Still, the expression of NLRP3 was increased after 24 h of LPS intervention. It was hypothesized that there may be some mechanisms against the activation of the NLRP3 inflammasome in the cell, which is worthy of further exploration. NLRP3 plays a critical role in the initiation of pyroptosis; hence, the present study used MCC950, an inhibitor of NLRP3, as a novel positive control to assess the effects of irisin *in vivo*. The characteristics of the mechanisms of action of irisin and MCC950 were compared. MCC950 inhibited LPS-induced neutrophil infiltration in lung tissue to a similar extent as Dex, an anti-inflammatory and immunosuppressant synthetic glucocorticoid, and decreased IL-1 β and IL-18 protein expression levels (2). In a previous study, MCC950 inhibited the secretion of IL-1 β in murine bone marrow-derived macrophages and NLRP3-induced apoptosis-associated speck-like protein containing a caspase recruitment domain oligomerization (44). The results of the present study confirmed that irisin and MCC950 downregulated the expression of IL-1 β and IL-18 in mouse serum and BALF. Additionally, irisin inhibited TNF- α production, whereas MCC950 did not. Western blot analysis and RT-qPCR revealed that irisin significantly inhibited the activation of HSP90, reduced the production and release of NLRP3, and inhibited downstream caspase-1 and GSDMD expression, indicating a different mechanism of action for irisin and MCC950.

HSP90, involved in the signaling pathway associated with the pyroptosis of AMs, is a potential target for anti-inflammatory drugs (2). Furthermore, the regulation of the stability of NLRP3 and the modulation of inflammasome activation by HSP90 is associated with IL-1 β secretion and pyroptosis (15). Therefore, it was considered that irisin inhibits the activation of HSP90 and interrupts the assembly of NLRP3, thus inhibiting pyroptosis and exerting anti-inflammatory effects. To examine the association between irisin and HSP90 *in vitro*, 17-AAG was used as a positive control. The results confirmed that 17-AAG, an inhibitor of HSP90, reduced the stability of NLRP3. Reportedly, it reduces the cleavage of caspase-1 and GSDMD in macrophages, thereby inhibiting pyroptosis (2). *In vitro* experiments revealed that irisin and 17-AAG were more effective in inhibiting the activation and release of caspase-1 and significantly reduced the expression of GSDMD, IL-1 β , and IL-18 following the co-incubation of MH-S cells with LPS. However, the decrease in TNF- α levels induced by 17-AAG treatment was not as pronounced as that induced by irisin, suggesting that irisin reduced the production and release of TNF- α through other signaling pathways. However, further studies are required to elucidate the underlying pathways and elucidate the precise mechanisms of action of irisin.

The present study has certain limitations. Targeted experiments to examine the expression of irisin in the lungs were not

conducted. The authors plan to design experiments to further explore the mechanisms through which FNDC5/irisin is expressed in injured lung tissue, as well as its clinical application in ALI.

In conclusion, the pyroptosis of AMs produces and releases pro-inflammatory cytokines in LPS-induced ALI. Irisin acts as an HSP90 inhibitor, regulating AM pyroptosis and exerting anti-inflammatory effects. Collectively, irisin regulates macrophage typing and inhibits the pyroptosis of AMs by regulating the HSP90/NLRP3/caspase-1/GSDMD pathway, downregulating the expression of inflammasomes and the release of pro-inflammatory cytokines. Irisin can be used as a novel treatment for ALI, and HSP90 may be a novel target with which inhibit the occurrence of pyroptosis.

Acknowledgements

The authors would like to thank the Hebei Key Laboratory of Vascular Homeostasis and the Hebei Collaborative Innovation Center for Cardio-Cerebrovascular Disease, Shijiazhuang, China for providing all the facilities to conduct the study.

Funding

The present study was supported by the Natural Science Foundation of Hebei Province (grant no. H2019206263); the Key R&D Program of Hebei Province (grant no. 19277760D); and the Hebei Province Applied Basic Research Program (grant no. 15967753D).

Availability of data and materials

The datasets used and/or analyzed during the current study are available from the corresponding author on reasonable request.

Authors' contributions

All authors participated in the design and interpretation of the study, in the analysis of the data and in the review of the manuscript. ZH, JM and AM designed the study, interpreted the data and revised the manuscript critically. ZH and JM conducted the majority of the experiments, performed the statistical analysis and wrote the manuscript. RJ, YH and GY conducted parts of the experiments. All authors have read and approved the final manuscript. YH and AM confirm the authenticity of all the raw data.

Ethics approval and consent to participate

The animal experimental and handling procedures were approved by the Ethics Committee of the Second Hospital of Hebei Medical University (Approval no. 2022-AE008, 2.28.2022). All experimental processes were carried out according to the National Institutes of Health Guide for the Care and Use of Laboratory Animals.

Patient consent for publication

Not applicable.

Competing interests

The authors declare that they have no competing interests.

References

1. Wheeler AP and Bernard GR: Acute lung injury and the acute respiratory distress syndrome: A clinical review. *Lancet* 369: 1553-1564, 2007.
2. Zhou Z, Li X, Qian Y, Liu C, Huang X and Fu M: Heat shock protein 90 inhibitors suppress pyroptosis in THP-1 cells. *Biochem J* 477: 3923-3934, 2020.
3. Kovacs SB and Miao EA: Gasdermins: Effectors of pyroptosis. *Trends Cell Biol* 27: 673-684, 2017.
4. Shi J, Zhao Y, Wang K, Shi X, Wang Y, Huang H, Zhuang Y, Cai T, Wang F and Shao F: Cleavage of GSDMD by inflammatory caspases determines pyroptotic cell death. *Nature* 526: 660-665, 2015.
5. Fan EK and Fan J: Regulation of alveolar macrophage death in acute lung inflammation. *Respir Res* 19: 50, 2018.
6. Martin WJ II, Wu M and Pasula R: A novel approach to restore lung immunity during systemic immunosuppression. *Trans Am Clin Climatol Assoc* 116: 221-227, 2005.
7. Murray PJ, Allen JE, Biswas SK, Fisher EA, Gilroy DW, Goerdt S, Gordon S, Hamilton JA, Ivashkiv LB, Lawrence T, *et al*: Macrophage activation and polarization: Nomenclature and experimental guidelines. *Immunity* 41: 14-20, 2014.
8. Gordon S, Plüddemann A and Martinez Estrada F: Macrophage heterogeneity in tissues: Phenotypic diversity and functions. *Immunol Rev* 262: 36-55, 2014.
9. Xu J, Jiang Y, Wang J, Shi X, Liu Q, Liu Z, Li Y, Scott MJ, Xiao G, Li S, *et al*: Macrophage endocytosis of high-mobility group box 1 triggers pyroptosis. *Cell Death Differ* 21: 1229-1239, 2014.
10. Li Z, Scott MJ, Fan EK, Li Y, Liu J, Xiao G, Li S, Billiar TR, Wilson MA, Jiang Y and Fan J: Tissue damage negatively regulates LPS-induced macrophage necroptosis. *Cell Death Differ* 23: 1428-1447, 2016.
11. Yang J, Zhao Y, Zhang P, Li Y, Yang Y, Yang Y, Zhu J, Song X, Jiang G and Fan J: Hemorrhagic shock primes for lung vascular endothelial cell pyroptosis: Role in pulmonary inflammation following LPS. *Cell Death Dis* 7: e2363, 2016.
12. He X, Qian Y, Li Z, Fan EK, Li Y, Wu L, Billiar TR, Wilson MA, Shi X and Fan J: TLR4-upregulated IL-1 β and IL-1RI promote alveolar macrophage pyroptosis and lung inflammation through an autocrine mechanism. *Sci Rep* 6: 31663, 2016.
13. Mayor A, Martinon F, De Smedt T, Pétrilli V and Tschopp J: A crucial function of SGT1 and HSP90 in inflammasome activity links mammalian and plant innate immune responses. *Nat Immunol* 8: 497-503, 2007.
14. Davis BK, Wen H and Ting JP: The inflammasome NLRs in immunity, inflammation, and associated diseases. *Annu Rev Immunol* 29: 707-735, 2011.
15. Piippo N, Korhonen E, Hytti M, Skottman H, Kinnunen K, Josifovska N, Petrovski G, Kaarniranta K and Kauppinen A: Hsp90 inhibition as a means to inhibit activation of the NLRP3 inflammasome. *Sci Rep* 8: 6720, 2018.
16. Zhang M, Liu L, Lin X, Wang Y, Li Y, Guo Q, Li S, Sun Y, Tao X, Zhang D, *et al*: A translocation pathway for vesicle-mediated unconventional protein secretion. *Cell* 181: 637-652.e615, 2020.
17. Wu X and Rapoport TA: Mechanistic insights into ER-associated protein degradation. *Curr Opin Cell Biol* 53: 22-28, 2018.
18. Ruggiano A, Foresti O and Carvalho P: Quality control: ER-associated degradation: Protein quality control and beyond. *J Cell Biol* 204: 869-879, 2014.
19. Huh JY, Panagiotou G, Mougios V, Brinkoetter M, Vamvini MT, Schneider BE and Mantzoros CS: FNDC5 and irisin in humans: I. Predictors of circulating concentrations in serum and plasma and II. mRNA expression and circulating concentrations in response to weight loss and exercise. *Metabolism* 61: 1725-1738, 2012.
20. Rabiee F, Lachinani L, Ghaedi S, Nasr-Esfahani MH, Megraw TL and Ghaedi K: New insights into the cellular activities of Fndc5/Irisin and its signaling pathways. *Cell Biosci* 10: 51, 2020.
21. Xiong XQ, Geng Z, Zhou B, Zhang F, Han Y, Zhou YB, Wang JJ, Gao XY, Chen Q, Li YH, *et al*: FNDC5 attenuates adipose tissue inflammation and insulin resistance via AMPK-mediated macrophage polarization in obesity. *Metabolism* 83: 31-41, 2018.
22. Mazur-Bialy AI, Pocheć E and Zarawski M: Anti-inflammatory properties of irisin, mediator of physical activity, are connected with TLR4/MyD88 signaling pathway activation. *Int J Mol Sci* 18: 701, 2017.
23. Shao L, Meng D, Yang F, Song H and Tang D: Irisin-mediated protective effect on LPS-induced acute lung injury via suppressing inflammation and apoptosis of alveolar epithelial cells. *Biochem Biophys Res Commun* 487: 194-200, 2017.
24. National Research Council (NRC): Institute for laboratory animal research: Guide for the care and use of laboratory animals. 8th edition. National Academies Press, Washington, DC, 2011.
25. Livak KJ and Schmittgen TD: Analysis of relative gene expression data using real-time quantitative PCR and the 2(-Delta Delta C(T)) method. *Methods* 25: 402-408, 2001.
26. Griffin RJ, Williams BW, Bischof JC, Olin M, Johnson GL and Lee BW: Use of a fluorescently labeled poly-caspase inhibitor for in vivo detection of apoptosis related to vascular-targeting agent arsenic trioxide for cancer therapy. *Technol Cancer Res Treat* 6: 651-654, 2007.
27. Cursio R, Colosetti P, Auberger P and Gugenheim J: Liver apoptosis following normothermic ischemia-reperfusion: In vivo evaluation of caspase activity by FLIVO assay in rats. *Transplant Proc* 40: 2038-2041, 2008.
28. Gill SE, Rohan M and Mehta S: Role of pulmonary microvascular endothelial cell apoptosis in murine sepsis-induced lung injury in vivo. *Respir Res* 16: 109, 2015.
29. Wang L, Lei W, Zhang S and Yao L: MCC950, a NLRP3 inhibitor, ameliorates lipopolysaccharide-induced lung inflammation in mice. *Bioorg Med Chem* 30: 115954, 2021.
30. Yokoyama S, Cai Y, Murata M, Tomita T, Yoneda M, Xu L, Pilon AL, Cachau RE and Kimura S: A novel pathway of LPS uptake through syndecan-1 leading to pyroptotic cell death. *Elife* 7: e37854, 2018.
31. Chen X, He WT, Hu L, Li J, Fang Y, Wang X, Xu X, Wang Z, Huang K and Han J: Pyroptosis is driven by non-selective gasdermin-D pore and its morphology is different from MLKL channel-mediated necroptosis. *Cell Res* 26: 1007-1020, 2016.
32. Fink SL and Cookson BT: Caspase-1-dependent pore formation during pyroptosis leads to osmotic lysis of infected host macrophages. *Cell Microbiol* 8: 1812-1825, 2006.
33. Lv H, Liu Q, Wen Z, Feng H, Deng X and Ci X: Xanthohumol ameliorates lipopolysaccharide (LPS)-induced acute lung injury via induction of AMPK/GSK3 β -Nrf2 signal axis. *Redox Biol* 12: 311-324, 2017.
34. Hughes KT and Beasley MB: Pulmonary manifestations of acute lung injury: More than just diffuse alveolar damage. *Arch Pathol Lab Med* 141: 916-922, 2017.
35. Nahrendorf M and Swirski FK: Abandoning M1/M2 for a network model of macrophage function. *Circ Res* 119: 414-417, 2016.
36. Jiang R, Xu J, Zhang Y, Zhu X, Liu J and Tan Y: Ligustrazine alleviate acute lung injury through suppressing pyroptosis and apoptosis of alveolar macrophages. *Front Pharmacol* 12: 680512, 2021.
37. Benoit M, Desnues B and Mege JL: Macrophage polarization in bacterial infections. *J Immunol* 181: 3733-3739, 2008.
38. Man SM, Karki R and Kanneganti TD: Molecular mechanisms and functions of pyroptosis, inflammatory caspases and inflammasomes in infectious diseases. *Immunol Rev* 277: 61-75, 2017.
39. Frank D and Vince JE: Pyroptosis versus necroptosis: Similarities, differences, and crosstalk. *Cell Death Differ* 26: 99-114, 2019.
40. Sun X, Sun J, Dong B, Huang G, Zhang L, Zhou W, Lv J, Zhang X, Liu M, Xu L, *et al*: Noninvasive temperature monitoring for dual-modal tumor therapy based on lanthanide-doped up-conversion nanocomposites. *Biomaterials* 201: 42-52, 2019.
41. Aggarwal NR, King LS and D'Alessio FR: Diverse macrophage populations mediate acute lung inflammation and resolution. *Am J Physiol Lung Cell Mol Physiol* 306: L709-L725, 2014.
42. He WT, Wan H, Hu L, Chen P, Wang X, Huang Z, Yang ZH, Zhong CQ and Han J: Gasdermin D is an executor of pyroptosis and required for interleukin-1 β secretion. *Cell Res* 25: 1285-1298, 2015.
43. Luo D, Dai W, Feng X, Ding C, Shao Q, Xiao R, Zhao N, Peng W, Yang Y, Cui Y, *et al*: Suppression of lncRNA NLRP3 inhibits NLRP3-triggered inflammatory responses in early acute lung injury. *Cell Death Dis* 12: 898, 2021.
44. Coll RC, Robertson AA, Chae JJ, Higgins SC, Muñoz-Planillo R, Isnera MC, Vetter I, Dungan LS, Monks BG, Stutz A, *et al*: A small-molecule inhibitor of the NLRP3 inflammasome for the treatment of inflammatory diseases. *Nat Med* 21: 248-255, 2015.



This work is licensed under a Creative Commons Attribution-NonCommercial-NoDerivatives 4.0 International (CC BY-NC-ND 4.0) License.